

Physical processes and biological productivity in the upwelling regions of the tropical Atlantic

Peter Brandt^{1,2}, Gaël Alory³, Founi Mesmin Awo⁴, Marcus Dengler¹, Sandrine Djakouré⁵, Rodrigue Anicet Imbol Koungue¹, Julien Jouanno³, Mareike Körner¹, Marisa Roch¹, Mathieu Rouault^{4,†}

¹GEOMAR Helmholtz Centre for Ocean Research Kiel, Kiel, Germany

²Faculty of Mathematics and Natural Sciences, Kiel University, Kiel, Germany

³LEGOS, CNES/CNRS/IRD/UPS, Toulouse, France

⁴Nansen-Tutu Centre for Marine Environmental Research, Department of Oceanography, University of Cape Town, Cape Town, South Africa

⁵LASMES, UFR SSMT, Felix Houphouët-Boigny University, Abidjan, Côte d'Ivoire

[†]deceased

Correspondence to: Peter Brandt (pbrandt@geomar.de)

Abstract

In this paper, we review observational and modelling results on the upwelling in the tropical Atlantic between 10°N and 20°S. We focus on the physical processes that drive the seasonal variability of surface cooling and upward nutrient flux required to explain the seasonality of biological productivity. We separately consider the equatorial upwelling system, the coastal upwelling system of the Gulf of Guinea and the tropical Angolan upwelling system. All three tropical Atlantic upwelling systems have in common a strong seasonal cycle with peak biological productivity during boreal summer. However, the physical processes driving the upwelling vary between the three systems. For the equatorial regime, we discuss the wind forcing of upwelling velocity and turbulent mixing as well as the underlying dynamics responsible for thermocline movements and current structure. The coastal upwelling system in the Gulf of Guinea is located along its northern boundary and is driven by both local and remote forcing. Particular emphasis is placed on the Guinea Current, its separation from the coast, and the shape of the coastline. For the tropical Angolan upwelling, we show that this system is not driven by local winds, but instead results from the combined effect of coastally trapped waves, surface heat and freshwater fluxes, and turbulent mixing. Finally, we review recent changes in the upwelling systems associated with climate variability and global warming and address possible responses of upwelling systems in future scenarios.

Short summary

Tropical upwelling systems are among the most productive ecosystems globally. The tropical Atlantic upwelling undergoes a strong seasonal cycle that is forced by the wind. Local wind-driven upwelling and remote effects particularly via the propagation of equatorial and coastal trapped waves lead to an up- and downward movement of the nitracline. Turbulent mixing results in upward supply of nutrients. Here, we review the different physical processes responsible for biological productivity.

1 Introduction

The tropical oceans are important to the Earth system for several reasons. The ocean receives a large part of shortwave radiation from the sun arriving at the Earth's surface that must be redistributed horizontally and vertically. Similar important exchanges of carbon dioxide, oxygen and other trace gases occur at the interface between tropical ocean and overlying atmosphere. Tropical marine ecosystems are among the most productive ones, with high relevance for global fisheries (Longhurst, 1993). They are associated with a substantial carbon

hat gelöscht: inner

hat gelöscht: primary

hat gelöscht: northern

hat gelöscht: concentrated

hat gelöscht: ,

hat gelöscht: The particular role of

hat gelöscht: nonlinearity

hat gelöscht: are emphasized

hat gelöscht: wind-

hat gelöscht: seasonal cycle of the zonal wind along the equator and the near-coastal wind field off Africa. Besides the wind forcing that lead to an up- and downward movement of the nitracline, turbulent diffusion results in upward mixing of nutrients. Here, we review the different physical processes responsible for upward nutrient supply.

flux from the near-surface into the deep ocean (Kiko et al., 2017). At the same time, the tropical oceans are affected by modes of natural climate variability that have reverberations around the globe, e.g., including the Pacific El Niño or the Atlantic Niño. Climate warming and change are thought to profoundly affect the tropical oceans. On the one hand, they impact natural climate variability via an intensification of climate extremes or changes in natural variability (Cai et al., 2018; Crespo et al., 2022; Prigent et al., 2020b; Yang et al., 2022). On the other hand, they are thought to **change the wind forcing of tropical oceans (Wang et al., 2015; Bakun, 1990)** or enhance stratification thereby impacting subduction, upwelling, and air-sea gas exchange with consequences for acidification, deoxygenation (Oschlies et al., 2018) and marine ecosystems.

The zonal extent of the tropical Atlantic is similar to that of the Indian Ocean and about three times smaller than that of the Pacific Ocean. The difference in size between the Pacific and Atlantic oceans seems to be the main reason for the dominance of interannual climate variability in the tropical Pacific, while the tropical Atlantic has largest variability on seasonal time scales (Keenlyside and Latif, 2007; Burls et al., 2011). **Moreover, the annual and semiannual cycles of primary production are strongly enhanced in the tropical Atlantic compared to the tropical Pacific** (Mao et al., 2020). A geographical peculiarity of the tropical Atlantic Ocean is the existence of the Gulf of Guinea which, in addition to its eastern boundary, **boards to the African continent in the north**, approximately along 5°N from 10°W to 10°E. There are several major rivers **flowing** into the tropical Atlantic including the Amazon, Congo and Niger rivers (Fig. 1).

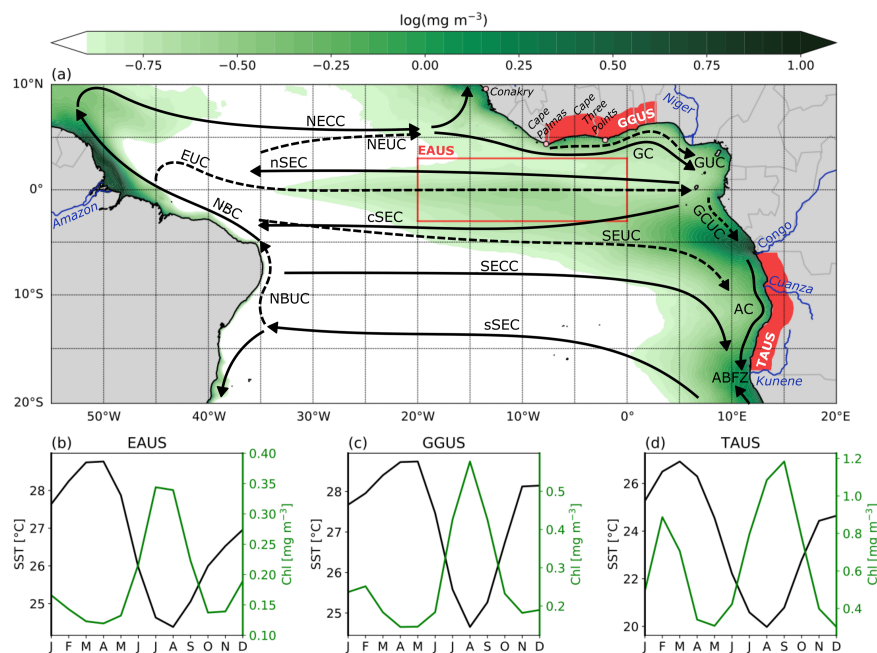


Fig. 1 (a) Mean chlorophyll concentration in the tropical Atlantic with circulation schematic superimposed. Surface (solid arrows) and thermocline (dashed arrows) current branches shown are the North Equatorial Countercurrent (NECC), the North Equatorial Undercurrent (NEUC), the Guinea Undercurrent (GUC), the Guinea Current (GC), the North Brazil Undercurrent (NBUC), the North Brazil Current (NBC), the Equatorial Undercurrent (EUC), the northern, central and southern branches of the South Equatorial Current (nSEC, cSEC, and sSEC), the South Equatorial Undercurrent (SEUC), the South Equatorial Countercurrent (SECC), the Gabon-

hat gelöscht:

hat gelöscht: ing of

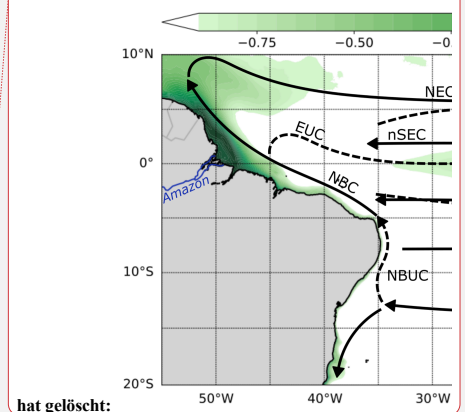
hat gelöscht: and

hat gelöscht: d

hat gelöscht: ,

hat gelöscht: also has a northern boundary extending

hat gelöscht: running



hat gelöscht:

hat gelöscht: Chlorophyll data are from Copernicus-GlobColour averaged for 1997-2022.

104 Congo Undercurrent (GCUC), and the Angola Current (AC). Also marked is the Angola-Benguela Frontal Zone
 105 (ABFZ) at about 17°S and the rivers Amazon, Niger, Congo, Cuanza, and Kunene. The red box marks the
 106 equatorial Atlantic upwelling system (EAUS, 20°W-0°, 3°N-3°S). Red patches mark the coastal extent of the Gulf
 107 of Guinea upwelling system (GGUS, 8°W-3°E, 1°-width coastal band) and the tropical Angolan upwelling system
 108 (TAUS, 6°-17°S, 1°-width coastal band). The mean seasonal cycle of SST and Chlorophyll is shown for EAUS
 109 (b), GGUS (c), and TAUS (d). SST data are from the Microwave OI SST product and Chlorophyll data are from
 110 Copernicus-GlobColour both averaged for 1998-2020.

112 Based on satellite data, Longhurst (1993) provided a first systematic overview of the different
 113 open ocean and coastal upwelling systems in the tropical Atlantic. Today, mean satellite
 114 chlorophyll concentration (Fig. 1) reveals enhanced productivity in the different coastal
 115 upwelling regions of the tropical Atlantic such as in the Gulf of Guinea upwelling system
 116 (GGUS, here defined as 8°W-3°E, 1°-width coastal band) and in the tropical Angolan upwelling
 117 system (TAUS, here defined as 6°-17°S, 1°-width coastal band). South of the TAUS, the
 118 permanent northern Benguela upwelling system is located with the Kunene upwelling cell at
 119 about 17°S forming its northern boundary (Siegfried et al., 2019). The equatorial Atlantic
 120 upwelling system (EAUS, here defined as 20°W-0°, 3°N-3°S) is an open ocean upwelling
 121 region, characterized by albeit enhanced but in comparison to the coastal upwelling systems
 122 relatively weak chlorophyll concentration (note the logarithmic scale for the chlorophyll
 123 concentration in Fig. 1) (Grodsky et al., 2008). Nevertheless, the EAUS is still of major
 124 importance for the overall biological productivity in the tropical Atlantic due to its large oceanic
 125 extent. Besides the tropical upwelling systems, enhanced chlorophyll concentration is found in
 126 the regions of the Amazon and the Congo river mouths. In the region of the Niger River mouth
 127 no comparable signal of enhanced chlorophyll is found likely due to much-reduced discharge
 128 of the Niger compared to the Amazon or Congo rivers (Fig. 1).

129 The tropical Atlantic upwelling is an element of the shallow overturning circulation, the
 130 subtropical cells (STCs), and is connected to the subduction in the eastern subtropics via
 131 equatorward thermocline flow and poleward Ekman transport in the surface layer (Schott et al.,
 132 2004; Fu et al., 2022; Tuchen et al., 2020). At the equator, the Equatorial Undercurrent (EUC)
 133 transports thermocline waters eastward, toward the EAUS. Due to the presence of the Atlantic
 134 meridional overturning circulation, these waters are almost exclusively of southern hemisphere
 135 origin (Schott et al., 1998; Johns et al., 2014; Tuchen et al., 2022a). Part of the waters
 136 recirculates into the westward current branches of the South Equatorial Current, the northern
 137 and the central South Equatorial Current, or contributes to supply the southward flow along the
 138 eastern boundary within the Gabon-Congo Undercurrent and the Angola Current
 139 (Kolodziejczyk et al., 2014; Kopte et al., 2017). The GGUS is supplied by the Guinea Current
 140 and the Guinea Undercurrent. While the waters of the Guinea Current mostly originate in the
 141 North Equatorial Countercurrent, a similar connection between the North Equatorial
 142 Undercurrent and the Guinea Undercurrent is less obvious (Bourlès et al., 2002; Djakouré et
 143 al., 2017; Herbert et al., 2016). Due to the much smaller width of the Atlantic compared to the
 144 Pacific, the thermocline waters arriving from the western boundary in the eastern basin
 145 upwelling systems are less enhanced in nitrate and less reduced in oxygen in the Atlantic
 146 compared to the Pacific (Brandt et al., 2015; Chai et al., 1996; Radenac et al., 2020).

147 The tropical Atlantic and its upwelling systems undergo a strong seasonal cycle (Fig. 1b-d).
 148 Main drivers are the seasonally varying winds associated with the meridional migration of the
 149 Intertropical Convergence Zone (ITCZ) (Fig. 2). During boreal summer, the ITCZ migrates
 150 northward resulting in strongly enhanced upwelling-favouring easterly winds along the equator
 151 and the establishment of the Atlantic cold tongue (ACT) centred around 10°W (Fig. 2c). The
 152 equatorial Atlantic is warmest in March/April (Fig. 2b) corresponding to a seasonal cycle with
 153 a fast cooling during the onset phase of the ACT and slower warming after it has reached its
 154 maximum spatial extent (Caniaux et al., 2011; Brandt et al., 2011). At the eastern boundary
 155 between equator and 15°S, lowest sea surface temperatures (SST) near the coast are found

hat gelöscht: strongly

hat nach unten verschoben [1]: in the region of the Amazon River and the Congo River mouths. In the region of the Niger River mouth no comparable signal of enhanced productivity is found likely due to its much-reduced discharge (Fig. 1). Besides the impact of river discharge on the mean chlorophyll concentration, high productivity is found

hat gelöscht: near the coasts in the Gulf of Guinea upwelling system (GGUS), and the tropical Angolan upwelling system (TAUS). ...

hat gelöscht: instead

hat gelöscht: to the

hat verschoben (Einfügung) [1]

hat gelöscht: area covered

hat gelöscht: River

hat gelöscht: R

hat gelöscht: productivity

hat gelöscht: its

hat gelöscht: Besides the impact of river discharge on the mean chlorophyll concentration, high productivity is found

hat gelöscht: Upwelling in the eastern tropical Atlantic is supplied by thermocline waters transported in different eastward currents.

hat gelöscht: es

hat gelöscht: ntertropical Convergence Zone

hat verschoben (Einfügung) [2]

hat gelöscht: in the eastern basin

Feldfunktion geändert

hat gelöscht: the

between July and September. At the northern boundary of the Gulf of Guinea, winds strengthen as well during boreal summer in accordance with northward migration of the ITCZ and the development of the West African Monsoon resulting in upwelling-favourable westerlies along the Ghanaian coast. Lowest SST near the coast is found in July-August (Fig. 2c).

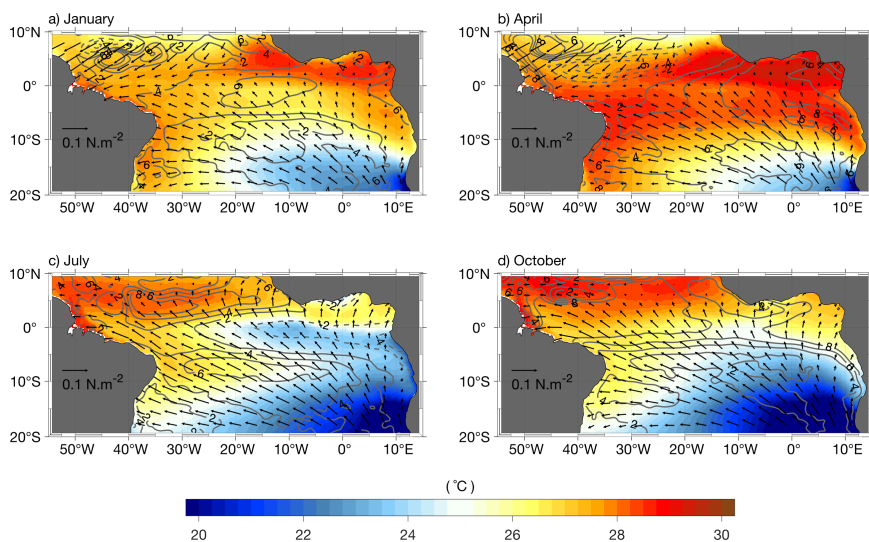


Fig. 2 Monthly mean sea surface temperature (SST, colour shading), sea level anomaly (contour lines, unit is cm), and wind stress (arrows) during (a) January, (b) April, (c) July and (d) October. SST data are from OI-SST (<https://www.esrl.noaa.gov/psd/data/gridded/>), surface wind stress from ERA5 (<https://cds.climate.copernicus.eu/>) and sea level anomalies from the European Union Copernicus Marine Service Information (<http://marine.copernicus.eu/>). The data are averaged between 1982-2021.

In the tropical Atlantic, the thermocline depth can often be associated with the depth of the nitracline. An upward movement of the thermocline thus marks upward vertical advection of nitrate fuelling biological productivity (Radenac et al., 2020). Besides local wind forcing, the propagation of equatorial and coastally trapped waves (CTWs) along the equatorial and coastal waveguides, respectively, contributes to the vertical movement of the thermocline/nitracline. Such wave propagation can result in dynamic upwelling far away from the wave generation sites (Illig et al., 2018b; Illig et al., 2018a; Bachélery et al., 2020; Hormann and Brandt, 2009). The Hovmöller diagrams of SST and winds as well as chlorophyll concentration and sea surface height show the seasonal development along the equatorial and coastal waveguides in the northern (Fig. 3) and southern (Fig. 4) hemispheres, respectively. Primary cooling in the EAUS can be identified following the enhancement of upwelling-favouring easterly winds along almost the whole equator in May-June (Weingartner and Weisberg, 1991). A secondary cooling occurs in November-December (Jouanno et al., 2011a; Okumura and Xie, 2006). In the GGUS, where SST reaches minimum values in August (Fig. 3a), upwelling-favouring westerly winds contribute to local cooling (Djakouré et al., 2017). Contrary, the southerly winds in the TAUS are particularly weak during phases of coldest sea surface (Fig. 4a) (Körner et al., 2022; Ostrowski et al., 2009). Biological productivity (or chlorophyll concentration) is generally enhanced during periods of depressed sea surface height or correspondingly during periods of elevated thermocline (Fig. 4b). In this review, we focus on the upper-ocean seasonal cycle in the three eastern-basin upwelling systems of the tropical Atlantic between about 10°N and 20°S, the physical forcing driving the

hat gelöscht:

hat nach oben verschoben [2]: The equatorial Atlantic is warmest in March/April (Fig. 2b) corresponding to a seasonal cycle with a fast cooling during the onset phase of the ACT and slower warming after it has reached its maximum spatial extent (Caniaux et al., 2011; Brandt et al., 2011).

hat gelöscht:

hat gelöscht: can

hat gelöscht: along the equator

hat gelöscht: Angolan upwelling region

hat gelöscht: marked by enhanced

hat gelöscht: 3

hat gelöscht: inner

upwelling, the upward nutrient supply, and the resulting biological productivity. Section 2 focusses on equatorial upwelling, section 3 on the Gulf of Guinea coastal upwelling and section 4 on the tropical Angolan upwelling. In section 5, we discuss longer-term changes and global warming and its relation to the seasonal cycle of upwelling, and, finally, in section 6, we provide a conclusion and outlook.

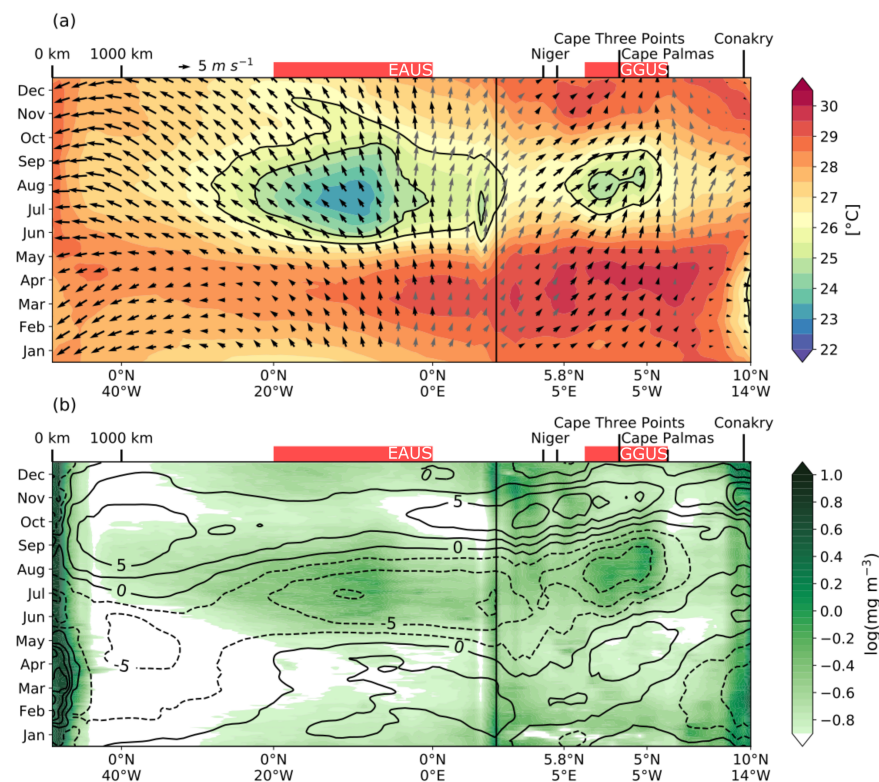
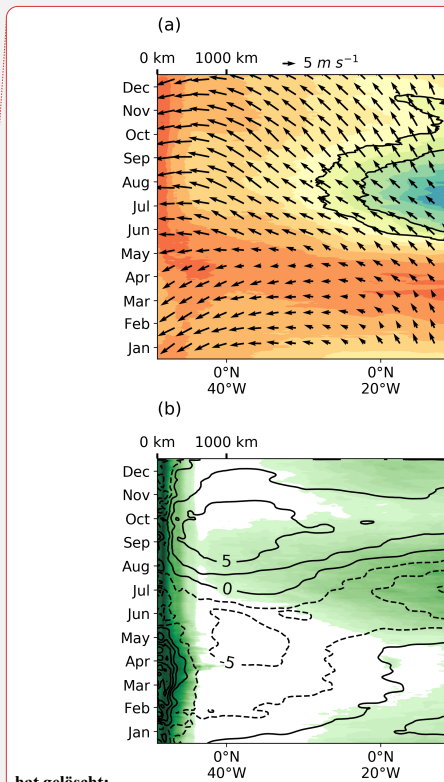


Fig. 3 Seasonal cycle of (a) sea surface temperature (shading) and wind stress (arrows) and (b) chlorophyll concentration (shading) and sea level anomaly (contour lines, unit is cm) along the equatorial (left of the vertical black lines) and Gulf of Guinea coastal waveguides (right of the vertical black lines). Marks at the lower x-axis give geographic coordinates and marks at the upper x-axis give a scale for the distance and geographic locations along the waveguides. Also included in (a) are contours of the 25°C and 26°C isotherms to highlight equatorial and coastal upwelling. Upwelling- and downwelling-favourable winds in (a) are marked by black and grey arrows, respectively. Upwelling-favourable winds have an eastward component along the equatorial waveguide and an alongshore-equatorward component along the coastal waveguide. Positive and negative sea level anomaly in (b) are marked by solid and dashed contour lines, respectively; mean sea level anomaly is removed. SST data are from the Microwave OI SST product, wind data are from CCMP, chlorophyll data are from Copernicus-GlobColour, sea level anomaly data are from Copernicus DUCAS. All data is averaged for 1998-2020 within a 1° band along the equator (+0.5°) and within 1° distance along the coast.

hat gelöscht: nitrate

hat gelöscht: implications of

hat gelöscht: for



hat gelöscht:

hat gelöscht: averaged for 1998-2022

hat gelöscht: ASCAT and QSCAT

hat gelöscht: averaged for 1991-2021

hat gelöscht: averaged for 1997-2022

hat gelöscht: averaged for 1993-2020

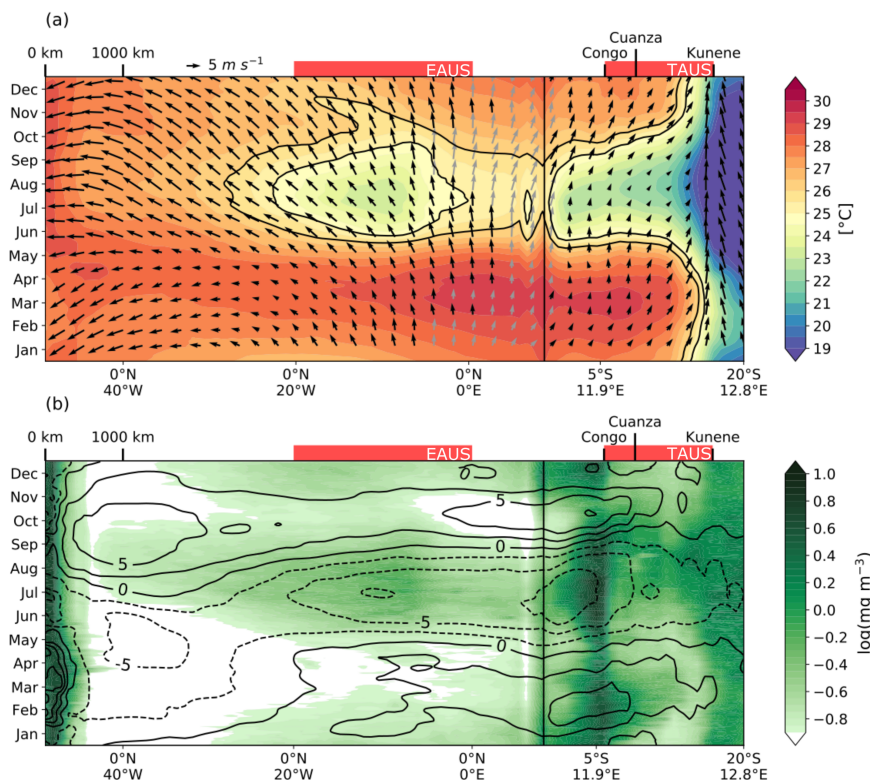
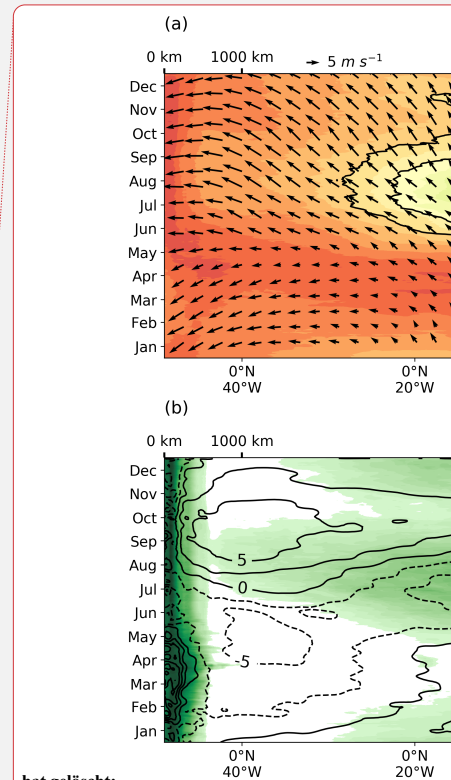


Fig. 4 Same as Fig. 3, but along the southwest African coastal waveguide (right of the vertical black lines).

2 Equatorial upwelling

The equatorial upwelling transports cool, nutrient-rich waters toward the surface of the equatorial Atlantic. Its influence at the surface is more pronounced in the eastern part of the basin, where it gives rise to the development of the ACT. Its intensity is modulated by a seasonal cycle composed of an annual and a semiannual component, with a primary SST minimum in July-August and a secondary minimum in November-December (Fig. 3) (Okumura and Xie, 2006; Jouanno et al., 2011a). First insights into the seasonal evolution were obtained from observational studies in the 1980s, revealing a close link between seasonal surface cooling and vertical movements of the thermocline (Merle, 1980; Voituriez et al., 1982). Indeed, periods of surface cooling in the eastern equatorial Atlantic are in phase with the thermocline upwelling in May-June and November (Fig. 5). By using forced ocean models, Philander and Pacanowski (1981) have revealed variations of the equatorial thermocline as forced by the seasonal cycle of the wind stress: stronger easterlies result in a stronger uplift of the thermocline in the eastern equatorial Atlantic. These authors discussed the response of the Atlantic Ocean to the seasonal wind forcing as an equilibrium response that can be understood as a succession of steady states. However, such an equilibrium response requires the dominance of low baroclinic mode equatorial Kelvin and Rossby waves that propagate fast enough to adjust the thermocline to the wind forcing within the seasonal cycle (Ding et al., 2009; Hormann and Brandt, 2009; Philander and Pacanowski, 1986, 1981). Beside the eastern thermocline uplift, the equatorial easterlies



hat gelöscht:

hat gelöscht: (Fig. 3)

hat gelöscht: s

force a strong eastward thermocline flow, the EUC, that supplies the upwelling in the eastern equatorial Atlantic (Johns et al., 2014; Schott et al., 1998). The equatorial upwelling is an integral part of the STCs that are driven by the easterlies away from the equator. The meridional divergence calculated from the Ekman transports at about 10°S and 10°N is about 20 Sv (Schott et al., 2004; Tuchen et al., 2019). Easterlies at the equator additionally result in equatorial upwelling that is part of the tropical cells (Perez et al., 2014). Tropical cells are similar overturning circulations as the STCs, but confined only to the upper 100 m with upwelling at the equator and downwelling at latitudes of about $\pm 3-5^\circ$. The annual mean tropical cells in the central tropical Atlantic are found to be asymmetric with respect to the equator; the northern cell extends into the southern hemisphere. This behaviour can be explained by the presence of southerly winds peaking during boreal autumn that drive a cross-equatorial northward surface flow at the equator (Heukamp et al., 2022). This circulation feature, often referred to as the equatorial roll, has maximum southward return flow at about 50 m depth and upwelling and downwelling slightly south and north of the equator, respectively. The upwelling velocity in the equatorial Atlantic is often estimated from local wind forcing as the sum of the Ekman pumping due to the zonal wind stress, meridional wind stress, wind stress divergence and wind stress curl (Caniaux et al., 2011). By using a realistic model of the equatorial Atlantic, particularly including the full dynamic response to the wind forcing, Giordani and Caniaux (2011) show that the dominant term driving the equatorial upwelling is still the forcing by zonal wind stress. The importance of the forcing by the wind stress divergence and the wind stress curl is, however, overestimated and underestimated, respectively, in the Ekman theory compared to the applied dynamic model. Over the past decade, several studies have revealed that turbulent mixing is the strongest cooling term of the mixed layer heat budget during the onset of the ACT and sets the spatial distribution and temporal variability of equatorial surface cooling (e.g., Jouanno et al., 2011a). Turbulent mixing at the base of the mixed layer that drives heat flux out of the mixed layer into the deeper ocean is dominantly induced by the vertical shear of the zonal equatorial currents, that is the westward South Equatorial Current at the surface and the eastward EUC at the thermocline level (Hummels et al., 2013). Different processes such as the seasonal variability in strength and core depth of the zonal currents, vertical shear associated with intraseasonal waves, the seasonally varying meridional circulation, and the deep-cycle turbulence contribute to the spatial and temporal variability of equatorial mixing (Moum et al., 2022; Heukamp et al., 2022). Using the diapycnal heat flux derived from observations, the seasonal mixed layer heat budget at the equator could be closed to a large extent and the seasonal development of the mixed layer temperatures reasonably well explained (Hummels et al., 2014). An important consequence of upwelling is the increase in biological productivity, that is primarily dependent on nitrate supply (Herbland and Voituriez, 1979; Loukos and Memery, 1999; Radenac et al., 2020; Moore et al., 2004). There is a strong similarity between the seasonal cycles of phytoplankton concentration and SST in the cold tongue area (Fig. 3) (Jouanno et al., 2011b), suggesting that the same physical processes control the downward heat flux out of the mixed layer and the upward supply of nitrate to the euphotic layer. This was confirmed by the analysis of repeated sections of PIRATA service cruises and outputs from a coupled physical-biogeochemical model (Radenac et al., 2020). Surface chlorophyll concentrations in the ACT peak in July-August and exhibit a secondary maximum in December-January (Figs. 3b and 4b, Fig. 5c). Radenac et al. (2020) showed that the primary phytoplankton bloom in July-August is due to a strong vertical nitrate input to the equatorial euphotic layer in May-July, and the secondary bloom in December is due to a shorter, moderate input in November-December (Fig. 5d). Their analysis of the nitrate balance in the upper ocean suggests that vertical advection controls the vertical movement of the nitracline and that vertical diffusion allows nitrate to reach the mixed layer (Figs. 5e, f). However, already noted by Monger et al. (1997), the phytoplankton concentration levels remain high beyond the primary

hat gelöscht: equatorial

hat gelöscht: in the Atlantic

hat gelöscht: , which defines the upwelling transport in the inner tropics,

hat gelöscht: latitude

hat gelöscht: In the Atlantic

hat gelöscht: t

hat gelöscht:

hat gelöscht: The different forcing terms of the upwelling velocity in the equatorial Atlantic are numerous and are discussed in detail in Giordani and Caniaux (2011). [f](#)

hat gelöscht: helps to defin

hat gelöscht: on

hat gelöscht: show

hat gelöscht: a

hat gelöscht: b

hat gelöscht: A

hat gelöscht: te input to the equatorial euphotic layer

hat gelöscht: c

hat gelöscht: d

bloom period in July-August, despite the fact that the thermocline/nitracline has dropped back to pre-uplift depth in September. Radenac et al. (2020) pointed towards a different behaviour of the EUC during boreal spring and autumn, where a shallow EUC during boreal spring might prevent upward mixing of nitrate compared to the deep phase of the EUC during boreal autumn, when nitrate more easily reaches into the shear zone above the EUC core (Fig. 5). However, also the equatorial role being at maximum strength during boreal autumn (Heukamp et al., 2022) might contribute to the nitrate supply into the mixed layer by upwelling slightly south of the equator.

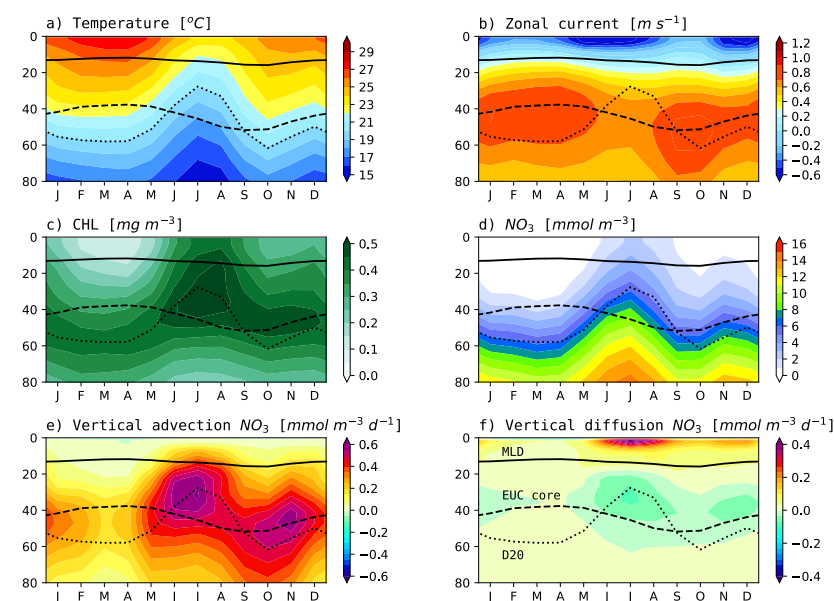
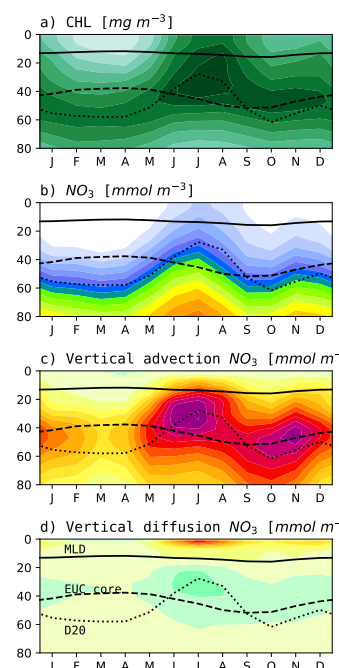


Fig. 5 Seasonal cycle of vertical profiles of (a) temperature, (b) zonal velocity, (c) chlorophyll, (d) nitrate, (e) vertical advection, and (f) vertical diffusion horizontally averaged in 1.5°S–0.5°N, 20–5°W. The depths of the mixed layer (upper solid line), of the EUC core (dashed line), and of the 20°C isotherm (dotted line) are indicated. Model output is taken from Radenac et al. (2020).

Analysis of the PIRATA shipboard sections and model outputs in Radenac et al. (2020) showed that waters transported eastward by the EUC have, in general relatively low nitrate concentrations compared to nearby water bodies to the north and south. This is most likely due to the source waters of the EUC that arrive from the oligotrophic layers of the subtropical South Atlantic (Schott et al., 1998; Johns et al., 2014; Tuchen et al., 2022a). The model simulations by Radenac et al. (2020) also revealed that the EUC core does not follow the thermocline depth (as defined as the 20°C isotherm, Fig. 5). While in the eastern equatorial Atlantic, the vertical migration of the thermocline undergoes a semiannual cycle in accordance with the local wind forcing, the EUC core depth has a dominant annual cycle (Brandt et al., 2014). This non-equilibrium response of the equatorial Atlantic to the seasonal wind forcing could be explained by resonant equatorial basin modes composed of eastward and westward propagating equatorial Kelvin and Rossby waves, respectively (Brandt et al., 2016). As the thermocline depth is a good proxy of the nitracline (Fig. 5d), the EUC transports elevated nitrate and phytoplankton concentrations when the EUC core is close to or deeper than the thermocline or nitracline, which is the case during July-August and to a lesser extent in December (Fig. 5).

hat gelöscht: Upwelling slightly south of the equator associated with southerly winds or turbulent mixing between EUC and South Equatorial Current were discussed to account for the enhanced nitrate concentration found above the EUC core during that period (Monger et al., 1997; Oudot and Morin, 1987).

Formatiert: Tabstops: 7,03 cm, Links



hat gelöscht:

hat gelöscht: b

hat gelöscht: c

Formatiert: Block

hat gelöscht: d

hat gelöscht:

hat gelöscht: s

hat gelöscht: s

hat gelöscht: s

hat gelöscht: , 6

hat gelöscht: b

hat gelöscht: nhanced

hat gelöscht: d

hat gelöscht: s

hat gelöscht: a, b

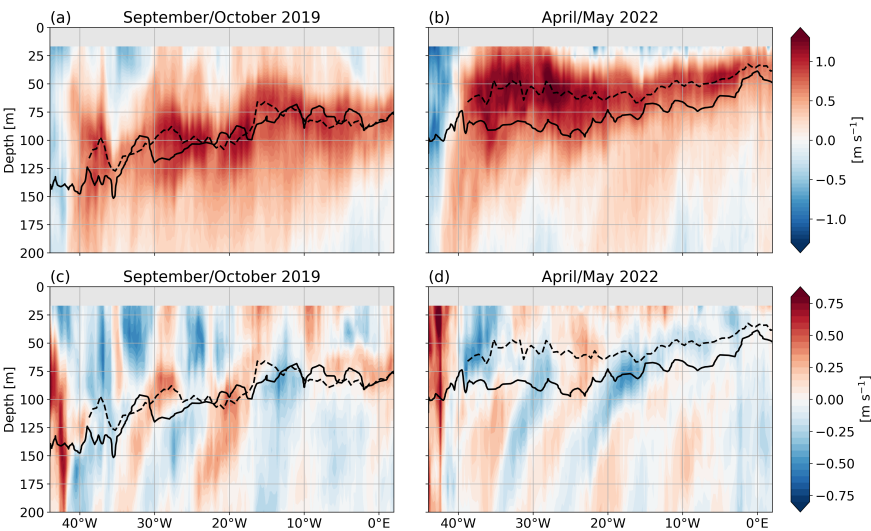


Fig. 6 Zonal (a, b) and meridional (c, d) velocity measured along the equator in September-October 2019 (a, c) and in April-May 2022 (b, d). Note, the different colour scales for the zonal and meridional velocities. EUC core depth is marked by dashed lines and the 20°C isotherm (as a proxy of the thermocline and the nitracline) by the solid lines.

Measurements along the equator during two cruises in boreal autumn (Fig. 6a) and boreal spring (Fig. 6b) reveal the basin-wide character of the up- and downward movement of the EUC core relative to the thermocline depths. During boreal autumn, the EUC core closely follows the thermocline, while during boreal spring, it is located clearly above the thermocline. This behaviour can be associated with the resonance of the equatorial basin at the annual period. The period of a resonant equatorial basin mode is given by the total travel time of an equatorial Kelvin wave and its reflected equatorial Rossby wave. For the width of the equatorial Atlantic basin, the resonance period of the 4th baroclinic mode is close to the annual cycle (Brandt et al., 2016). This basin mode is associated with maximum eastward velocity in the near-surface layer in boreal spring and maximum westward flow in boreal autumn. A specific consequence of the relative movement of EUC core and thermocline depths is that the thermocline and thus the nitracline during part of the year vertically migrates into the shear zone above the EUC core. As the upper shear zone of the EUC supports strongly elevated turbulent mixing (Hummels et al., 2014; Hummels et al., 2013; Jouanno et al., 2011b; Moum et al., 2022), enhanced upward nutrient flux occurs during those periods. Such behaviour was identified in the model study of Radenac et al. (2020) showing a maximum in the near-surface diffusive nitrate flux into the mixed layer in July-August and a secondary maximum in November-December (Fig. 5d). Beside a seasonal cycle, the productivity on the equator shows elevated intraseasonal and shorter-term variability. In particular, tropical instability waves (TIWs) and wind-forced intraseasonal waves play an important role in stimulating locally productivity due to both meridional advection of nitrate and chlorophyll as well as due to events of enhanced vertical advection and mixing (Athie and Marin, 2008; Menkes et al., 2002; Jouanno et al., 2013). TIWs are found to be associated with strong mixing events (Moum et al., 2009) or the generation of fronts (Warner et al., 2018) that both can drive upward nutrient supply. Resulting high

hat gelöscht: t equatorial basin mode of the
hat gelöscht: showing an annual cycle
hat gelöscht: (Brandt et al., 2016)

hat gelöscht: This was confirmed by
hat gelöscht: a
hat gelöscht: d

productivity events could be observed during the boreal autumn cruise (Figs. 6a, c) that took place shortly after the seasonal maximum of the TIW activity (Sherman et al., 2022).

3 Gulf of Guinea upwelling

In the Gulf of Guinea, coastal upwelling occurs seasonally along the northern coast, between 10°W and 5°E, from Côte d'Ivoire to Nigeria (Hardman-Mountford and McGlade, 2003). It plays a key role in primary production and local fisheries and is therefore of large socio-economic importance for the bordering countries (Koné et al., 2017; Amemou et al., 2020). SST variability in the GGUS is suggested to modulate the amplitude of the African monsoon and thus has influence on regional climate (Caniaux et al., 2011; Djakouré et al., 2017). The GGUS is composed of two main upwelling cells, an eastern cell east of Cape Three Points (4°44'N, 2°05'W) and a western cell east of Cape Palmas (4°22'N, 7°43'W), that are marked by regions of reduced SST near the coast in satellite data (Fig. 3a) (Wiawe and Nyadjro, 2015). Different physical processes have been proposed to explain the presence of the coastal upwelling in the GGUS. In early studies, the coastal upwelling has been related to the strengthening of the geostrophic coastal current by local and remote wind forcing. Indeed, the seasonal strengthening in the eastward-flowing Guinea Current contributes to enhance the meridional tilt of the thermocline, thereby bringing cooler subsurface waters near the coast closer to the surface (Colin et al., 1993; Ingham, 1970; Bakun, 1978; Philander, 1979). The link between SST and wind stress curl in the GGUS was first suggested by Katz and Garzoli (1982) and Garzoli and Katz (1983). By using a model of the tropical Atlantic, Philander and Pacanowski (1986) showed the influence of both wind components and the wind stress curl on the upwelling in the GGUS. Additionally, Marchal and Picaut (1977) analysed isotherm displacements between Ghana and Côte d'Ivoire and suggested that vertical pumping by cyclonic eddies generated downstream of Cape Three Points and Cape Palmas, could explain upwelling of cool waters. However, modelling results by Djakouré et al. (2014) did not confirm that the cyclonic eddies generated downstream of the capes contribute to the upwelling. Instead, Djakouré et al. (2014) and Djakouré et al. (2017) suggested that the upwelling downstream of Cape Palmas is associated with the nonlinear dynamics of the Guinea Current. The inclusion of the nonlinearity in the momentum equations of their model results in an inertial detachment of the Guinea Current from the coast after passing Cape Palmas. The geostrophic adjustment at the coastward flank of the current then leads to thermocline upwelling downstream of Cape Palmas. It is worth noting that the thermocline depth, the strength of the coastal current, and thus the upwelling, are all under the seasonal remote influence of the equatorial ocean through the propagation of equatorial Kelvin and Rossby waves as well as CTWs (Moore et al., 1978; Clarke, 1979; Servain et al., 1982; Picaut, 1983; Adamec and Obrien, 1978). Such remote influence is also indicated by the seasonal cycle of the sea level anomaly along the equatorial and coastal waveguides (Fig. 3b) and was found for intraseasonal wave propagations as well (Polo et al., 2008; Imbol Koungue and Brandt, 2021).

By using a model of the tropical Atlantic with an embedded high-resolution nest for the Gulf of Guinea, Djakouré et al. (2014) and Djakouré et al. (2017) performed sensitivity experiments to identify the dominant processes driving the seasonal upwelling in GGUS. The sensitivity includes experiments with a changed coastline without the capes (Djakouré et al., 2014) and with the nonlinear terms in the momentum equations responsible for the advection of momentum removed (Djakouré et al., 2017). The spatial distribution of the mean SST for the major upwelling season (July-September) is shown for their reference simulation in Fig. 7. A comparison of the sensitivity experiments with the reference simulations (Fig. 8) shows that the sea surface during boreal summer is still colder than the 25°C (chosen as a threshold for the presence of coastal upwelling), when the capes are removed (Fig. 8b). The western upwelling

hat gelöscht: constituted

hat gelöscht: clearly

hat gelöscht: the

hat gelöscht: capes

hat gelöscht: and its

hat gelöscht: and

hat gelöscht: (Bakun, 1978)

cell disappears only when the nonlinear terms **in the momentum equations** are removed and the Guinea Current is trapped at the coast (Fig. 8c). The thermocline depth, superimposed on the SST in Fig. 8, is in each of these configurations closest to the surface during the upwelling season. During this period, in the simulation without capes, the thermocline has a structure almost identical to that of the realistic configuration. However, the thermocline depth is always larger than 20 m in the simulation without capes and thus deeper than in the reference simulation. In the simulation without nonlinear terms, the **deepening of the thermocline relative to the reference simulation is stronger** in the western upwelling cell than in the eastern upwelling cell (west and east of Cape Three Points, respectively) **resulting in strongly reduced cooling in the western upwelling cell when advection of momentum is removed**. The sensitive experiments demonstrated that advection of momentum is the main contributor to the vertical pumping of the western upwelling cell; the cooling of the eastern upwelling cell is mainly associated with the **offshore Ekman transport** (Djakouré et al., 2017).

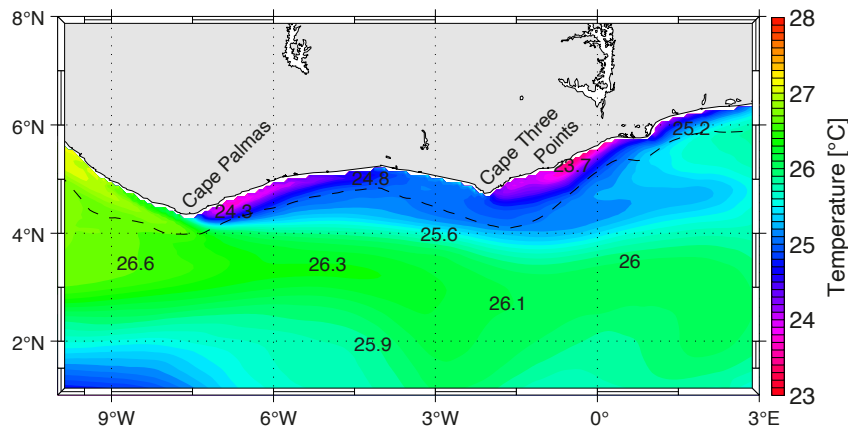


Fig. 7 Mean SST (°C) for the major cold season (July - September) of the reference experiment by Djakouré et al. (2017). The dashed line represents the 1000 m isobath. **Model output is taken from Djakouré et al. (2017).**

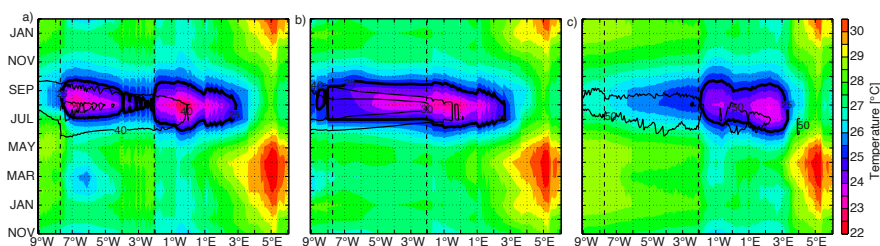


Fig. 8 Hovmöller diagrams of SST (°C) along the coast of the GGUS from 9°W to 6°E of (a) the reference experiment, the idealized experiments (b) without capes and (c) without inertial terms. The thermocline depth (20°C isotherm) is superimposed (thin contour lines, unit is m). The vertical dashed black lines represent the longitude of Cape Palmas and Cape Three Points, see Fig. 7. The time axis in months extends from November to February of the following year. The 25°C isotherm is additionally marked to highlight the coastal upwelling (thick contour lines). **Model output is taken from Djakouré et al. (2014) and Djakouré et al. (2017).**

hat gelöscht: while generally deeper than in the reference simulation,

hat gelöscht: is closer to the surface

hat gelöscht: while

hat gelöscht: wind-induced coastal divergence

hat gelöscht: for

In the eastern part of the GGUS that is dominantly wind-driven (Fig. 3a), coastal cooling weakens toward the east while approaching the Niger River mouth (Fig. 9). Earlier studies have shown that onshore geostrophic flow can compensate wind-driven offshore transport, thus reducing upwelling in some regions (Marchesiello and Estrade, 2010; Rossi et al., 2013). Using a realistic regional model configuration, Ekman and geostrophic coastal upwelling indices were compared to coastal vertical velocities along the northern Gulf of Guinea coast, during the boreal summer season (Alory et al., 2021). Indeed, the upwelling indices were able to explain a large part of vertical velocity variations along the coast. They also showed that wind-forced coastal upwelling is reduced by about 50% due to onshore geostrophic flow east of 1°E (Fig. 9a). Note that the Ekman coastal upwelling index shown in Fig. 9a only takes into account the Ekman transport, as Ekman pumping has little influence in this region (Wiafe and Nyadjro, 2015). The onshore geostrophic flow is associated with a sea level slope increasing toward the east. It is driven by density differences along the coast, from relatively cool and salty waters in the upwelling core east of Cape Three Points (Fig. 7) to warm and fresh waters in the Niger River plume and largely compensates offshore Ekman transport and therefore reduces upwelling (Fig. 9a). The comparison of a reference simulation with a simulation in which river run-off is removed, revealed that the Niger River discharge contributes to induce an onshore geostrophic surface flow, but additionally causes a thinning of the mixed layer. Overall, there is no net effect of the river discharge on the near-surface geostrophic transport from which the geostrophic upwelling index is derived. Nevertheless, the Niger River discharge induces a coastal warming reaching 1°C near 2°E (Fig. 9b), which likely is the result of reduced turbulent mixing by the enhanced salt stratification (Alory et al., 2021). The summer upwelling season corresponds both to a maximum thinning of the mixed layer and maximum surface chlorophyll concentration along the coast (Toualy et al., 2022). Riverine nutrient inputs may be more or less compensated by a reduced upward nutrient flux due to discharge-driven increased stratification as there is no strong chlorophyll signal in the plume region (Fig. 1).

hat gelöscht: dynamical

hat gelöscht: all

hat gelöscht: found to be

hat gelöscht: a weakening of

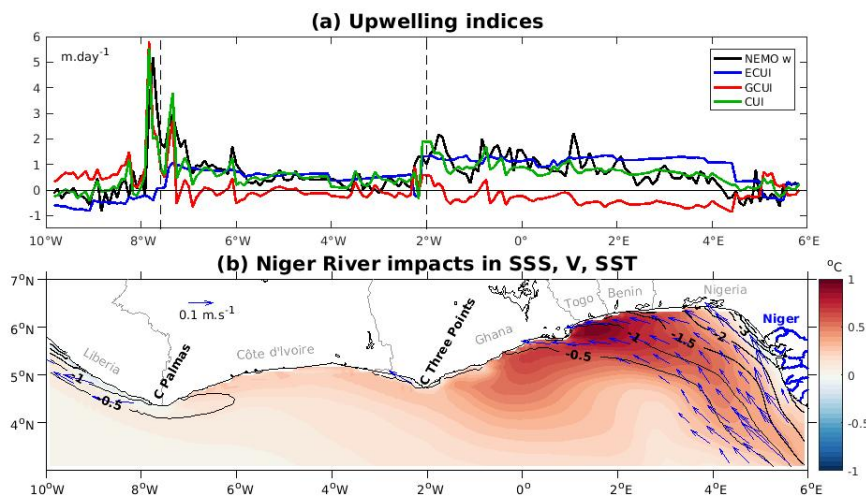


Fig. 9 (a) Climatological mean (2010-2017) boreal summer (July - September) coastal upwelling index (CUI, green line), defined as the sum of Ekman (ECUI, blue line) and geostrophic (GCUI, red lines) coastal upwelling indices, compared with coastal vertical velocity at the base of the mixed layer in the reference NEMO simulation (black line). Correlation between the CUI and vertical velocities is 0.72. Vertical dashed lines indicate the location

hat gelöscht: G

of Cape Palmas and Cape Three Points. (b) River effects on boreal summer sea surface salinity (contour lines), surface geostrophic current (arrows) and sea surface temperature (colour shadings), from a difference between the NEMO reference and a runoff-free simulation. Model output is taken from Alory et al. (2021).

4 Tropical Angolan upwelling

The Angolan waters host a highly productive ecosystem: the **TAUS** (Fig. 1). Located in the southern hemisphere between the Congo River mouth at 6°S and the Angola-Benguela frontal zone at **about 17°S**, the **TAUS** is of great socio-economic importance for local communities. Fishing supplies about 25% of the total animal protein intake of the Angolan population and is critical for economic security (Hutchings et al., 2009; Sowman and Cardoso, 2010; FAO, 2022). The productivity in the **TAUS** undergoes a distinct seasonal cycle (Fig. 4). In the **TAUS** during austral winter, maximum productivity is observed at the same time as the lowest SST and the strongest cross-shore temperature gradient are present (Tchpalanga et al., 2018; Awo et al., 2022; Körner et al., 2022). In contrast to other eastern boundary upwelling systems, the seasonality of the productivity in the **TAUS** cannot be explained by local wind forcing (Ostrowski et al., 2009). Prevailing southerly winds in the **TAUS** are generally weak throughout the year (Fig. 4a). Neither the seasonal cycle of alongshore wind stress nor of the wind stress curl are in phase with the seasonal cycle in productivity suggesting that other mechanisms drive the productivity seasonality in the **TAUS** (Körner et al., 2022).

One of the key dynamics modulating the **TAUS** on different time scales is the passage of CTWs (Bachelery et al., 2016a; Kopte et al., 2018; Kopte et al., 2017; Illig et al., 2018b; Tchpalanga et al., 2018; Awo et al., 2022; Körner et al., 2022). CTWs that propagate poleward along the eastern boundary are forced remotely by wind fluctuations along the equator or locally by winds at the eastern boundary. Sea level satellite observations reveal the seasonal passage of four remotely forced CTWs throughout the year (Fig. 4b) (Rouault, 2012; Tchpalanga et al., 2018). A downwelling CTW **marked by anomalously high sea level** arrives at the Angolan coast in March followed by an upwelling CTW **marked by anomalously low sea level** in June/July. A secondary downwelling CTW propagates along the Angolan coast in October followed by a secondary upwelling CTW in December/January. The main component of the eastern boundary circulation in the **TAUS** is the poleward Angola Current (Kopte et al., 2017; Siegfried et al., 2019). Its variability is linked to equatorial ocean dynamics via the propagations of CTWs at different time scales (Kopte et al., 2018; Kopte et al., 2017; Imbol Koungue and Brandt, 2021). On seasonal time scales the **poleward** velocities of the Angola Current peak in October with a secondary maximum in February (Kopte et al., 2017).

The hydrographic conditions in the **TAUS** undergo distinct seasonal changes (Fig. 10). Conductivity, temperature, depth (CTD) data from fifteen years of biannual research cruises of the Nansen program (Tchpalanga et al., 2018) illustrate the seasonal differences between the primary downwelling phase in **late** austral summer and the primary upwelling phase in austral winter (Fig. 10). In **late** austral summer (February-April) the cross-shelf section derived from data averaged between 10°S and 12°S shows warm surface waters and a subsurface salinity maximum **below low-salinity surface water**. The subsurface salinity maximum is absent in austral winter (June-August). The isopycnals show evidence of down- and upwelling as they bend downward towards the shore in **late** austral summer and upward in austral winter. Furthermore, the isopycnals undergo a vertical displacement between the seasons (the 26.2 kg m⁻³ isopycnal moves vertically by about 50 m). The vertical displacement of the permanent thermocline can be attributed to the passage of CTWs. The seasonal passage of four CTWs induces a semiannual cycle in the vertical isopycnal movements (Kopte et al., 2017; Rouault, 2012).

hat gelöscht: tAUS

hat gelöscht: 5

hat gelöscht: tAUS

hat gelöscht: tAUS

hat gelöscht: tAUS

hat gelöscht: tAUS

hat gelöscht: tAUS

hat gelöscht: tAUS

hat gelöscht: tAUS

hat gelöscht: tAUS

hat gelöscht: south

hat gelöscht: tAUS

hat gelöscht:

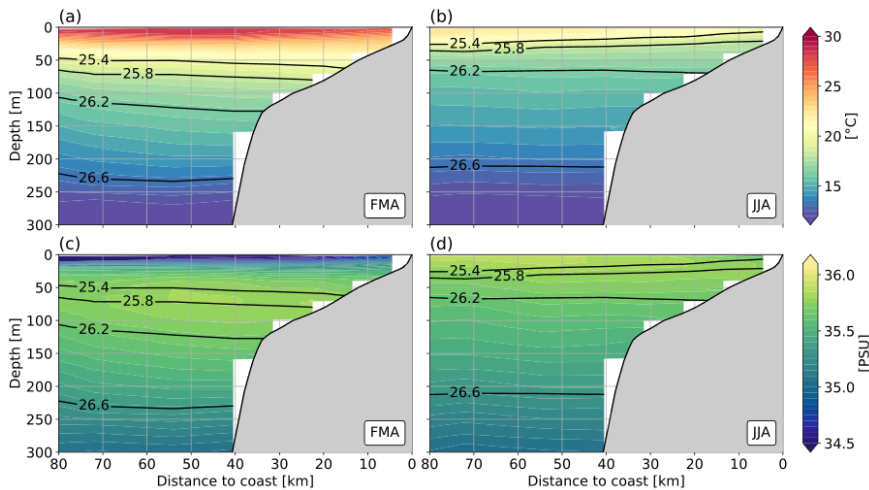


Fig. 10 Hydrographic conditions between 10°S and 12°S during main downwelling phase, February-April (a,c) and main upwelling phase, June-August (b,d) inferred from the Nansen CTD dataset (Tchpalanga et al., 2018). CTD data is projected on mean topography (GEBCO) between 10°S and 12°S. Panels a and b show the temperature field, panels c and d the salinity field. Black contour lines mark potential density.

To understand the changes in SST in the **TAUS**, one has to account for other processes than the passage of CTWs. The SST which shows an annual cycle is dominantly driven by the surface heat fluxes. The advection of warm water by the Angola Current plays only a minor role (Körner et al., 2022). In the **TAUS**, SST is reduced in a narrow strip along the coast compared to further offshore (Fig. 2). The resulting negative cross-shore SST gradient has a semiannual cycle and is strongest between April and September, with a secondary maximum in December/January. The cross-shore SST gradient can neither be explained by surface heat fluxes which act to dampen the spatial SST differences nor by the weak horizontal heat advection. Ocean turbulence data revealed that turbulent mixing across the base of the mixed layer is strongest in shallow waters (water depths smaller than 75 m) and capable of setting up the negative cross-shore SST gradient. The semiannual cycle of the gradient can be explained by turbulent mixing acting upon seasonally different stratifications (Körner et al., 2022) as discussed below.

In contrast to SST, sea surface salinity (SSS) in the **TAUS** undergoes a semiannual cycle. Fresher water is found in the northern part of the **TAUS** in October/November and in February/March (Fig. 10) (Kopte et al., 2017; Lübbecke et al., 2019; Awo et al., 2022). An important source of freshwater in the **TAUS** is the Congo River discharge at 6°S, with a maximum discharge into the ocean in early December (Martins and Stammer, 2022). The observed freshwater in the **TAUS** is controlled by meridional advection via the Angola Current and peaks in phase with the strengthening of the Angola Current (Awo et al., 2022). Indeed, the Angola Current displaces the freshwater from the Congo River plume toward the **TAUS**, leading to elevated stratification with low-salinity water at the surface above a subsurface salinity maximum. This strong stratification favours the subsurface advection of high salinity water counteracting surface freshening via vertical salt advection and mixing at the base of the mixed layer (Awo et al., 2022).

Turbulent mixing is an important mechanism in the **TAUS** for the near-coastal cooling, upward salt flux, and upward nutrient supply (Awo et al., 2022; Ostrowski et al., 2009; Körner et al., 2022). Ocean turbulence data from six research cruises is used to analyse the distribution of vertical eddy diffusivity at a cross-shelf section at 11°S (Fig. 11). The vertical eddy diffusivity

hat gelöscht: tAUS

hat gelöscht: tAUS

hat gelöscht: lower

hat gelöscht: are found

hat gelöscht: directly

hat gelöscht: tAUS

hat gelöscht: tAUS

hat gelöscht: tAUS

hat gelöscht: tAUS

hat gelöscht: tAUS

hat gelöscht: tAUS

is elevated near the bottom at the continental slope and shelf. Additionally, waters shallower than 75 m show enhanced diffusivities over nearly the whole water column. This finding suggests a dependence of mixing on bathymetry in the TAUS with stronger mixing occurring in shallow waters, similar to other upwelling systems (Schafstall et al., 2010; Perlin et al., 2005).

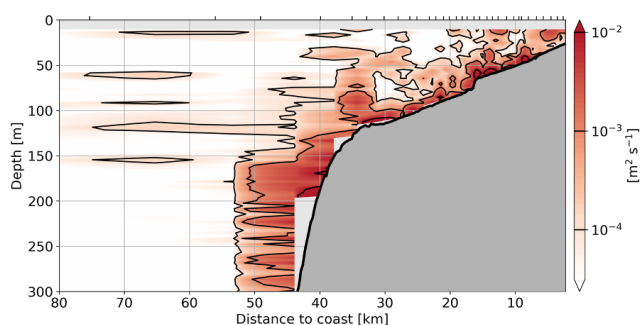


Fig. 11 Vertical eddy diffusivity calculated from microstructure observation as a function of depth and distance to the coast. Measurements are taken at a section at about 11°S. Eddy diffusivity is calculated for each profile individually before profiles are binned together in groups of 20 profiles (black ticks on top mark the border of the 20-profile groups).

The elevated mixing rates in shallow waters of the TAUS can be explained by onshore propagating internal waves interacting with sloping topography. The main energy source of the internal wave field is assumed to be internal tides, which are generated by the interaction of the barotropic tide and the continental slope (Hall et al., 2013; Lamb, 2014). By applying a regional general circulation model forced solely by barotropic tides at the open boundaries, Zeng et al. (2021) found that in the TAUS a substantial part of the tidally generated internal wave energy propagates onshore and dissipates in shallow waters. Resulting enhanced near-shore mixing agrees well with observations. The seasonality of the spatially-averaged generation, onshore flux, and dissipation of internal tide energy is weak. This means that throughout the year, roughly the same amount of energy is available for mixing in shallow waters. However, the resulting mixing acts on seasonally different background stratifications that vary due to the passage of CTWs as well as due to surface heat and freshwater fluxes (Körner et al., 2022; Kopte et al., 2017). Zeng et al. (2021) showed that variations in the background stratification led to different effects of mixing on temperature: the sea surface in shallow waters near the coast is cooling, stronger during phases of weak stratification than during phases of strong stratification. The productivity season in the TAUS is in phase with the propagation of CTWs (Fig. 4). The chlorophyll concentration peaks around one month after the passage of the primary upwelling CTW in austral winter. Similarly, a secondary chlorophyll peak is visible after the passage of the secondary upwelling CTW in December/January (Figs. 1 and 4). However, the exact process of how the passage of the CTWs leads to an increase in primary production remains an open question. While the sea surface cooling depends on the background stratification (Zeng et al., 2021; Körner et al., 2022), the upward nutrient supply additionally depends on the background distribution of nutrients. An increased vertical nitrate gradient during phases of upwelling CTW in areas of high mixing would result in higher upward nitrate fluxes. Such changes in the background nitrate conditions associated with upward and onshore advection of nitrate during the passage of upwelling CTWs might be able to ultimately explain the seasonal productivity signals in the TAUS.

5 Relation between upwelling seasonality and longer-term variability

hat gelöscht: tAUS

hat gelöscht: ly

hat gelöscht: tAUS

hat gelöscht: the interaction between

hat gelöscht: and

hat gelöscht: numerical

hat gelöscht: tAUS

hat gelöscht: energy available for

hat gelöscht: leading to different effects of mixing on temperature ...

hat gelöscht: Associated with the passage of CTWs as well as with changes in surface heat fluxes and SSS, the stratification in the tAUS undergoes a semiannual cycle (Kopte et al., 2017).

hat gelöscht: how cooling in

hat gelöscht: near coastal area is

hat gelöscht: tAUS

hat gelöscht: seasonal

hat gelöscht: The seasonal varying effect of mixing on SSTs shows that a reduction in stratification can lead to more effective cooling near the coast during the upwelling phase

hat gelöscht: .

hat gelöscht: T

hat gelöscht: change in the

hat gelöscht: H

hat gelöscht: nutrient

hat gelöscht: could be achieved by increasing the nutrient gradient during phases of upwelling CTW in areas of high mixing...

hat gelöscht: the

hat gelöscht: nutrients

hat gelöscht: tAUS

The seasonal upwelling in the three upwelling systems discussed here peaks approximately during the same period, i.e., in July-September (Fig. 1b-d). The area and season most impacted by the upwelling show marked interannual variability, whether in terms of SST (Keenlyside and Latif, 2007) or phytoplankton concentration (Chenillat et al., 2021). Fig. 12 shows the year-to-year variability of SST of the three tropical Atlantic upwelling systems averaged for the three months July-September. There are some similarities but also differences in the variability of the three upwelling systems. Outstanding is the most recent warm event in 2021 that peaks in all three upwelling systems.

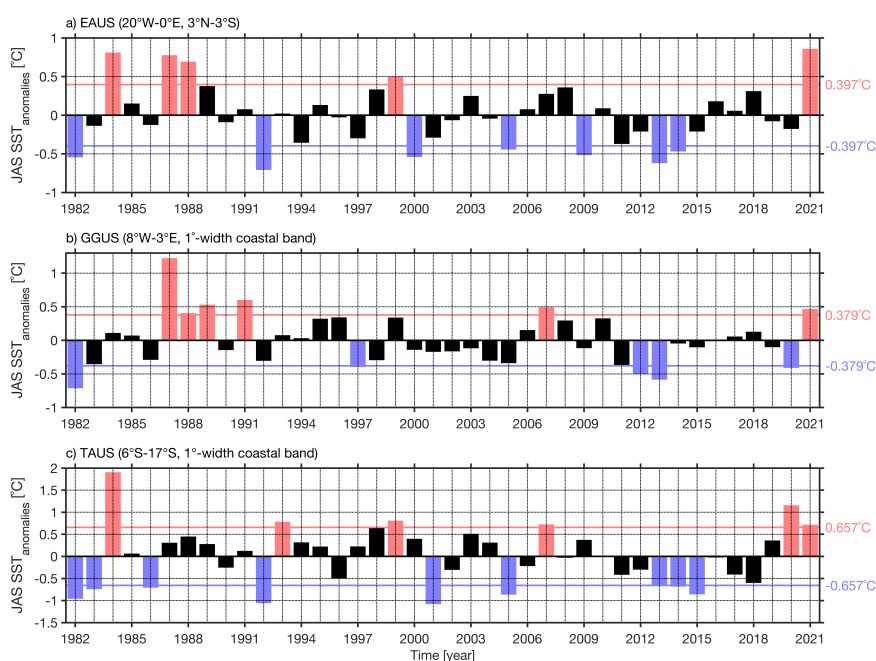


Fig. 12 SST anomalies from 1982-2021 during the main upwelling season (July-September) averaged in the EAUS (a), GGUS (b), and TAUS (c). The red and blue rectangles highlight the extreme warm and cold events in the different regions, respectively. The horizontal red and blue lines show the standard deviation of the interannual SST anomalies during the main upwelling season (July-September). Anomalies are derived with respect to the seasonal cycle between 1982 and 2021 after subtracting the trend. SST data are from OI-SST (<https://www.esrl.noaa.gov/psd/data/gridded/>).

The dominant climate mode in the tropical Atlantic is the Atlantic Niño (Hisard, 1980; Ruiz-Barradas et al., 2000; Lübbecke et al., 2018). It is most pronounced in the equatorial cold tongue east of 23°W and peaks during June-July (Keenlyside and Latif, 2007). Anomalous warm or cold events are thus associated with anomalous deep or shallow thermocline and correspondingly with reduced or enhanced upwelling, respectively. Atlantic Niños and Niñas are associated with SSS variability as well (Awo et al., 2018) suggesting additional forcing of the equatorial and eastern boundary upwelling in the eastern tropical Atlantic as the coupling between subsurface and surface is reduced for enhanced near-surface stratification. During an Atlantic Niño, the southward shift of the ITCZ brings maximum rainfall in the eastern tropical Atlantic and potentially increases the flow of surrounding rivers, affecting near-surface

hat gelöscht: has important consequences on the expression of the interannual variability at the sea surface of the tropical Atlantic

hat gelöscht: It is t

hat gelöscht: that

hat gelöscht: boreal summer

hat gelöscht: The

hat gelöscht: is

hat gelöscht: an

hat gelöscht: ly

795 stratification (Awo et al., 2018; Nyadjro et al., 2022). Besides the interannual variability,
 796 decadal variability can impact the equatorial upwelling. Such variability might be associated
 797 with a changing strength of the STCs forced by off-equatorial easterlies (Rabe et al., 2008;
 798 Tuchen et al., 2020). Similarly, Brandt et al. (2021) found an intensification of the EUC for the
 799 period 2008-2018 that was linked to enhanced trade winds in the tropical North Atlantic likely
 800 associated with the Atlantic multidecadal variability (Knight et al., 2006). Other mechanisms
 801 that are suggested to impact the strength of equatorial cooling on decadal time scales include
 802 the decadal variability of TIWs. A decadal strengthening of TIWs was found to be associated
 803 with enhanced warming of the equatorial cold tongue by lateral eddy fluxes (Tuchen et al.,
 804 2022b). Coupled climate simulations also suggest the importance of surface heat fluxes in
 805 driving interannual to decadal cold tongue SST variability (Nnamchi et al., 2015). As discussed
 806 by Jouanno et al. (2017), such heat flux forcing is likely overemphasized due to large upper
 807 ocean temperature biases commonly found in climate models. Chang et al. (2008) analysed the
 808 impact of a changing Atlantic meridional overturning circulation (AMOC) on the tropical
 809 Atlantic on decadal to multidecadal timescales using simulations with a climate model. These
 810 simulations showed that a weakened AMOC results in a warmer equatorial Atlantic with
 811 reduced seasonal cycle and interannual variability. Similarly, a weakening of interannual
 812 variability is projected under a global warming scenario (Crespo et al., 2022; Yang et al., 2022).
 813 However, the impact of global warming or reduced AMOC on seasonal or interannual
 814 variability of productivity is highly uncertain as even the impact on upper ocean stratification
 815 is not coherent between different models and datasets, which is partly due to the fact that
 816 decadal trends in stratification or productivity are just emerging from the available observations
 817 (Roch et al., 2021; Sallee et al., 2021; Hammond et al., 2020).
 818 In the GGUS, interannual variability is generally stronger in regions of strong seasonal
 819 variability as has been documented from satellite and in situ data (Wiafe and Nyadjro, 2015;
 820 Sohoun et al., 2020). Potential drivers of interannual variability are similar to drivers of seasonal
 821 changes. They include changes in the wind forcing and turbulent mixing, and remote forcing
 822 associated with the Atlantic Niño (Jouanno et al., 2017; Wade et al., 2011). Processes involved
 823 in the 2012 cold anomalies in the GGUS, one of the coldest events observed over the last 30
 824 years (Fig. 12b), have been investigated through a model heat budget (Da-Allada et al., 2021).
 825 Results revealed that the surface cooling at Cape Palmas was driven by changes in zonal
 826 advection and increased turbulent mixing due to a strengthening of the Guinea Current and
 827 associated vertical shear, while east at Cape Three Point, where seasonal upwelling is
 828 dominated by the wind forcing, it was driven by a strengthening of the zonal wind stress that
 829 increased the offshore Ekman transport.
 830 In the TAUS, Benguela Niños and Niñas are the dominant modes of interannual climate
 831 variability (Shannon et al., 1986). Contrary to the variability in the EAUS and GGUS,
 832 interannual variability does not reach its seasonal maximum during the main upwelling season,
 833 but during the main downwelling season from March-May (Lübbecke et al., 2019). Still, some
 834 events are observed during austral winter such as the 1984 Benguela Niño (Imbol Koungue et
 835 al., 2019; Shannon et al., 1986). During a Benguela Niño or Niña, SST in the TAUS can be up
 836 to 2°C higher or lower than the climatology, respectively (Rouault et al., 2007; Rouault et al.,
 837 2018; Imbol Koungue et al., 2019; Imbol Koungue et al., 2021). These extreme events can have
 838 drastic consequences for the marine ecosystem (Gammelsrød et al., 1998) through modulations
 839 in coastal upwelling intensity, nutrients and oxygen content along the continental shelf
 840 (Bachelery et al., 2016b). It can be assumed that forcing mechanisms of Benguela Niños and
 841 Niñas are similar to those of the seasonal upwelling variability. On the one hand, winds at the
 842 equator can generate equatorial Kelvin waves (Illig et al., 2004) that continue southward along
 843 the southwest African coast as CTWs and produce thermocline displacements along the eastern
 844 boundary (Polo et al., 2008; Imbol Koungue et al., 2017; Bachelery et al., 2016a; Bachelery et
 845 al., 2020). On the other hand, fluctuations of local alongshore winds (Richter et al., 2010) and

hat gelöscht: by the impact of precipitation and river discharge on near-surface stratification

hat gelöscht: first

hat gelöscht: in the tAUS

hat gelöscht: seasonally

hat gelöscht: to

hat gelöscht: in the tAUS

hat gelöscht: locally

other local processes such as freshwater inputs (Lübbecke et al., 2019) further generate SST anomalies in the **TAUS**. For the satellite era, Prigent et al. (2020a) showed a weakening of interannual SST variability in the southeastern tropical Atlantic between 2000-2017 relative to 1982-1999. However, since 2018, two consecutive extreme coastal warm events have been recorded in the **TAUS** in 2019/2020 (Imbol Koungue et al., 2021) and in 2021 (Fig. 12c). The recent decades demonstrate a strong warming trend in the tropical Atlantic SST with the largest warming observed in the coastal upwelling regions off southwestern Africa including the **TAUS** (Tokinaga and Xie, 2011). Moreover, using observational data, Roch et al. (2021) discovered a change in upper-ocean stratification from subtropical to tropical conditions associated with a warming and freshening of the mixed layer between 2006 and 2020 in the southeastern tropical Atlantic (10°S-20°S; 5°W-15°E). Such changes in stratification are assumed to particularly impact the mixing-driving nitrate supply in the **TAUS**.

6 Conclusion and outlook

Here we have reviewed the physical processes in three major upwelling systems of the tropical Atlantic (10°N-20°S), the EAUS, the GGUS, and the **TAUS**, that drive the upwelling seasonality. Among them are the processes that locally impact the thermocline depth - often used as a proxy of the nitracline - such as zonal wind along the equator, alongshore wind in coastal upwelling regions, wind stress curl or the detachment of the boundary current. Remote processes associated with the propagation of equatorial Kelvin and CTWs affect the thermocline depth in the different upwelling regions on intraseasonal, seasonal and interannual timescales as well. The processes affecting the thermocline depth can be summarized under locally and remotely driven vertical advection which is able to transfer colder and nutrient-rich waters upward to the surface during active upwelling. Additionally, diffusive fluxes associated with turbulent mixing at the base of the mixed layer and within the thermocline transport heat downward and nutrients upward. While the dominant processes driving equatorial and coastal upwelling might be identified, we are only beginning to quantify their relative importance or to understand their interactions. Examples are the nonlinear interaction of locally and remotely forced boundary current variability and horizontal density anomalies or topography (Mosquera-Vasquez et al., 2014; Kämpf, 2007), the importance and characteristics of different CTW modes and their specific role in the vertical advection of nutrients (Bachelery et al., 2020; Illig et al., 2018a; Illig et al., 2018b), or the role of intraseasonal variability and the eddy field in shaping the upwelling (Tuchen et al., 2022b; Thomsen et al., 2016). With the development of extremely high-resolution ocean models the importance of the mesoscale, submesoscale and their role in mixed layer dynamics and thermocline mixing emerged. Dedicated observational studies particularly in eastern boundary upwelling systems are required, focussing on these smaller-scale dynamics and aiming at understanding their impact on seasonal and longer-term changes of upwelling.

The EAUS can be characterized as a wind-driven upwelling system forced by different wind components at the equator and off the equator. Off-equatorial winds drive the STCs, which act on longer time-scales, mostly larger than 5 years (Schott et al., 2004; Tuchen et al., 2020). How their changes affect stratification and nutrient distribution is still an open question (Duteil et al., 2014). Wind changes along the equator generate upwelling and downwelling equatorial waves propagating along the equator and adjust the equatorial thermocline to reach an equilibrium with the wind forcing. Additional wave forcing originates from westward propagating Rossby waves and their reflection at the western boundary (Foltz and McPhaden, 2010a, b) or by CTWs generated at the western boundary (Hughes et al., 2019). A very specific response of an equatorial basin is the development of a basin resonance. Due to its width and the travel time of equatorial waves, the Atlantic basin is resonant at the 2nd and 4th baroclinic modes for the semi-annual and annual cycles, respectively. The resonance results in an EUC that vertically

hat gelöscht: tAUS

hat gelöscht: tAUS

hat gelöscht: tAUS

hat gelöscht: tAUS

hat gelöscht: inner

hat gelöscht: tAUS

hat gelöscht: and

hat gelöscht: in coastal upwelling regions

hat gelöscht: The zonal velocity field instead is dominated by the equatorial basin resonance of the 2nd and 4th baroclinic modes resulting

migrates largely independently of the thermocline (Brandt et al., 2016). During periods, when the thermocline depth is shallower than the EUC core, turbulent mixing in the shear zone above the core of the EUC is essential for the downward heat flux and upward nitrate flux out and into the mixed layer, respectively (Jouanno et al., 2011b; Hummels et al., 2014). Similar resonances are found for the Indian Ocean (Han et al., 2011), while the Pacific Ocean due to its larger width develops resonances at lower baroclinic modes and/or larger periods.

In the GGUS different processes define the two upwelling centres, east of Cape Palmas and east of Cape Three Points. East of Cape Palmas, the inertial detachment of Guinea Current from the coast plays the most important role, while east of Cape Three Points, upwelling is mainly associated with the wind-forced coastal divergence (Djakouré et al., 2017). The upwelling in the TAUS, which is characterized by weak winds, is dominantly driven by a combination of remotely forced CTWs and turbulent mixing locally enhanced in shallow waters near the coast (Körner et al., 2022; Tchipalanga et al., 2018; Rouault, 2012).

Climate warming and change might impact the upwelling in the different regions and their seasonality (amplitude and phase) differently. Most obvious are probably future changes in the wind field, e.g., a strengthening of the winds in a warming world or poleward shifts of the main wind systems (Yang et al., 2020). Changes in the stratification and mixed layer depths are highly uncertain with recent studies suggesting an increase of the stratification at the base of the mixed layer together with a mixed layer deepening likely due to enhanced wind-driven upper-ocean turbulent mixing (Sallee et al., 2021; Roch et al., 2021). However, other processes such as lateral mixing, responsible for reducing nitrate concentrations in upwelling regions, or surface heat fluxes, might contribute as well. Recently, the multidecadal increase in the strength of TIWs and associated equatorward eddy heat flux was suggested to warm the EAUS (Tuchen et al., 2022b). Such eddy fluxes generally oppose the Ekman transport in upwelling systems. Air-sea heat and buoyancy fluxes were identified to modulate such compensation in idealized model simulations (Thomsen et al., 2021), suggesting that in a warming climate also changes in heat and freshwater fluxes have the potential to impact the upwelling strength via its impact on lateral eddy fluxes.

The identification of climate changes in upwelling systems is a major goal that requires the maintenance and further development of the tropical Atlantic observing system (Foltz et al., 2019). In particular, coastal upwelling regions show a sparse data coverage and the strengthening of the near-coastal observing system has a high priority. This requires a close cooperation with the coastal communities to jointly develop the research agenda according to collective interests and needs. Main questions regard the often-competing role of changes in wind forcing and stratification and the role of changing eddy fluxes and buoyancy forcing. What will be the consequences of changing upwelling amplitude and/or timing for biogeochemistry and biology? Overall, future upwelling studies require a close cooperation between different research disciplines focussing on the interaction between the physical, biogeochemical and biological systems and allowing an improved assessment of ecosystem management and fisheries.

Data availability

Publicly available datasets were used for this study. Chlorophyll data (1998-2020) are from the Copernicus-GlobColour dataset (<https://doi.org/10.48670/moi-00281>). The sea level anomaly data (1998-2020) were accessed via the Copernicus Server (<https://doi.org/10.48670/moi-00148>). Microwave OI SST and CCMP wind data (both 1998-2020) are available under <https://www.remss.com>. Also used are surface wind stress from ERA5 (<https://cds.climate.copernicus.eu/>). Hydrographic sections in Angolan waters have been produced using the Nansen CTD Dataset (<https://doi.pangaea.de/10.1594/PANGAEA.887163>).

hat gelöscht: nonlinear

hat gelöscht: induced

hat gelöscht: tAUS

hat gelöscht: locally induced

hat gelöscht: its

hat gelöscht: <https://doi.org/10.48670/moi-00021>

hat gelöscht: from ASCAT and QSCAT

974 **Author contribution**

975
976 PB outlined and wrote the manuscript. MK, RI, JJ, SD, GA produced the figures. All co-authors
977 contributed to and reviewed the manuscript.
978

979 **Appendix A**

980
981 List of abbreviations.

982	AMOC	Atlantic meridional overturning circulation
983	ACT	Atlantic cold tongue
984	CTD	conductivity, temperature, depth
985	CTW	coastally trapped wave
986	EAUS	equatorial Atlantic upwelling system
987	EUC	Equatorial Undercurrent
988	FAO	Food and Agriculture Organization
989	GGUS	Gulf of Guinea upwelling system
990	ITCZ	Intertropical Convergence Zone
991	TAUS	tropical Angolan upwelling system
992	TIWs	tropical instability waves
993	SSS	sea surface salinity
994	SST	sea surface temperature
995	STC	subtropical cells

996
997 **Acknowledgements**

998
999 The study was funded by EU H2020 under grant agreement 817578 TRIATLAS project. It was
1000 further supported by the German Federal Ministry of Education and Research as part of the
1001 BANINO (03F0795A) project, [by the German Research Foundation through grant 511812462](#)
1002 [\(IM 218/1-1\), and by the French Research Institute for Development \(IRD\) as part of the JEAI](#)
1003 [IVOARE-UP project.](#)
1004

hat gelöscht: tAUS

References

- Adamec, D. and Obrien, J. J.: Seasonal upwelling in Gulf of Guinea due to remote forcing, *J Phys Oceanogr*, 8, 1050-1060, [https://doi.org/10.1175/1520-0485\(1978\)008<1050:Tsuitg>2.0.Co;2](https://doi.org/10.1175/1520-0485(1978)008<1050:Tsuitg>2.0.Co;2), 1978.
- Alory, G., Da-Allada, C. Y., Djakouré, S., Dadou, I., Jouanno, J., and Loemba, D. P.: Coastal Upwelling Limitation by Onshore Geostrophic Flow in the Gulf of Guinea Around the Niger River Plume, *Front Mar Sci*, 7, 607216, <https://doi.org/10.3389/fmars.2020.607216>, 2021.
- Amemou, H., Koné, V., Aman, A., and Lett, C.: Assessment of a Lagrangian model using trajectories of oceanographic drifters and fishing devices in the Tropical Atlantic Ocean, *Prog Oceanogr*, 188, 102426, <https://doi.org/10.1016/j.pocean.2020.102426>, 2020.
- Athie, G. and Marin, F.: Cross-equatorial structure and temporal modulation of intraseasonal variability at the surface of the Tropical Atlantic Ocean, *J Geophys Res-Oceans*, 113, C08020, <https://doi.org/10.1029/2007jc004332>, 2008.
- Awo, F. M., Rouault, M., Ostrowski, M., Tomety, F. S., Da-Allada, C. Y., and Jouanno, J.: Seasonal cycle of sea surface salinity in the Angola Upwelling System, *J Geophys Res-Oceans*, 127, e2022JC018518, <https://doi.org/10.1029/2022JC018518>, 2022.
- Awo, F. M., Alory, G., Da-Allada, C. Y., Delcroix, T., Jouanno, J., Kestenare, E., and Baloitcha, E.: Sea Surface Salinity Signature of the Tropical Atlantic Interannual Climatic Modes, *J Geophys Res-Oceans*, 123, 7420-7437, <https://doi.org/10.1029/2018jc013837>, 2018.
- Bachèlery, M. L., Illig, S., and Dadou, I.: Interannual variability in the South-East Atlantic Ocean, focusing on the Benguela Upwelling System: Remote versus local forcing, *J Geophys Res-Oceans*, 121, 284-310, <https://doi.org/10.1002/2015jc011168>, 2016a.
- Bachèlery, M. L., Illig, S., and Dadou, I.: Forcings of nutrient, oxygen, and primary production interannual variability in the southeast Atlantic Ocean, *Geophys Res Lett*, 43, 8617-8625, <https://doi.org/10.1002/2016gl070288>, 2016b.
- Bachèlery, M. L., Illig, S., and Rouault, M.: Interannual coastal trapped waves in the Angola-Benguela upwelling system and Benguela Niño and Niña events, *J Marine Syst*, 203, 103262, <https://doi.org/10.1016/j.jmarsys.2019.103262>, 2020.
- Bakun, A.: Guinea Current Upwelling, *Nature*, 271, 147-150, <https://doi.org/10.1038/271147a0>, 1978.
- Bakun, A.: Global Climate Change and Intensification of Coastal Ocean Upwelling, *Science*, 247, 198-201, <https://doi.org/10.1126/science.247.4939.198>, 1990.
- Bourlès, B., D'Orgeville, M., Eldin, G., Gouriou, Y., Chuchla, R., DuPenhoat, Y., and Arnault, S.: On the evolution of the thermocline and subthermocline eastward currents in the Equatorial Atlantic, *Geophys Res Lett*, 29, 32.31-32.34, <https://doi.org/10.1029/2002gl015098>, 2002.
- Brandt, P., Funk, A., Tantet, A., Johns, W., and Fischer, J.: The Equatorial Undercurrent in the central Atlantic and its relation to tropical Atlantic variability, *Clim Dynam*, 43, 2985-2997, <https://doi.org/10.1007/s00382-014-2061-4>, 2014.
- Brandt, P., Claus, M., Greatbatch, R. J., Kopte, R., Toole, J. M., Johns, W. E., and Böning, C. W.: Annual and semiannual cycle of equatorial Atlantic circulation associated with basin-mode resonance, *J Phys Oceanogr*, 46, 3011-3029, <https://doi.org/10.1175/Jpo-D-15-0248.1>, 2016.
- Brandt, P., Caniaux, G., Bourlès, B., Lazar, A., Dengler, M., Funk, A., Hormann, V., Giordani, H., and Marin, F.: Equatorial upper-ocean dynamics and their interaction with the West African monsoon, *Atmos Sci Lett*, 12, 24-30, <https://doi.org/10.1002/Asl.287>, 2011.
- Brandt, P., Hahn, J., Schmidtke, S., Tuchen, F. P., Kopte, R., Kiko, R., Bourlès, B., Czeschel, R., and Dengler, M.: Atlantic Equatorial Undercurrent intensification counteracts warming-

induced deoxygenation, *Nat Geosci*, 14, 278-282, <https://doi.org/10.1038/s41561-021-00716-1>, 2021.

Brandt, P., Bange, H. W., Banyte, D., Dengler, M., Didwischus, S. H., Fischer, T., Greatbatch, R. J., Hahn, J., Kanzow, T., Karstensen, J., Körtzinger, A., Krahmann, G., Schmidtke, S., Stramma, L., Tanhua, T., and Visbeck, M.: On the role of circulation and mixing in the ventilation of oxygen minimum zones with a focus on the eastern tropical North Atlantic, *Biogeosciences*, 12, 489-512, <https://doi.org/10.5194/bg-12-489-2015>, 2015.

Burls, N. J., Reason, C. J. C., Penven, P., and Philander, S. G.: Similarities between the tropical Atlantic seasonal cycle and ENSO: An energetics perspective, *J Geophys Res-Oceans*, 116, C11010, <https://doi.org/10.1029/2011jc007164>, 2011.

Cai, W. J., Wang, G. J., Dewitte, B., Wu, L. X., Santoso, A., Takahashi, K., Yang, Y., Carreric, A., and McPhaden, M. J.: Increased variability of eastern Pacific El Niño under greenhouse warming, *Nature*, 564, 201-206, <https://doi.org/10.1038/s41586-018-0776-9>, 2018.

Caniaux, G., Giordani, H., Redelsperger, J. L., Guichard, F., Key, E., and Wade, M.: Coupling between the Atlantic cold tongue and the West African monsoon in boreal spring and summer, *J Geophys Res-Oceans*, 116, C04003, <https://doi.org/10.1029/2010jc006570>, 2011.

Chai, F., Lindley, S. T., and Barber, R. T.: Origin and maintenance of a high nitrate condition in the equatorial Pacific, *Deep-Sea Res Pt II*, 43, 1031-1064, [https://doi.org/10.1016/0967-0645\(96\)00029-X](https://doi.org/10.1016/0967-0645(96)00029-X), 1996.

Chang, P., Zhang, R., Hazeleger, W., Wen, C., Wan, X. Q., Ji, L., Haarsma, R. J., Breugem, W. P., and Seidel, H.: Oceanic link between abrupt changes in the North Atlantic Ocean and the African monsoon, *Nat Geosci*, 1, 444-448, <https://doi.org/10.1038/Ngeo218>, 2008.

Chenillat, F., Illig, S., Jouanno, J., Awo, F. M., Alory, G., and Brehmer, P.: How do climate modes shape the Chlorophyll-a interannual variability in the tropical Atlantic?, *Geophys Res Lett*, 48, e2021GL093769, <https://doi.org/10.1029/2021GL093769>, 2021.

Clarke, A. J.: On the generation of the seasonal coastal upwelling in the Gulf of Guinea, *J Geophys Res-Oc Atm*, 84, 3743-3751, <https://doi.org/10.1029/JC084iC07p03743>, 1979.

Colin, C., Gallardo, Y., Chuchla, R., and Cissoko, S.: Environnements climatique et océanographique sur le plateau continental de Côte d'Ivoire, in: *Environnement et ressources aquatiques de Côte d'Ivoire : 1. Le milieu marin*, edited by: Le Loeuff, P., Marchal, E., and Amon Kothias, J. B., ORSTOM, Paris, 75-110, 1993.

Crespo, L. R., Prigent, A., Keenlyside, N., Koseki, S., Svendsen, L., Richter, I., and Sanchez-Gomez, E.: Weakening of the Atlantic Niño variability under global warming, *Nat Clim Change*, 12, 822-827, <https://doi.org/10.1038/s41558-022-01453-y>, 2022.

Da-Allada, C. Y., Agada, J., Balotcha, E., Hounkonnou, M. N., Jouanno, J., and Alory, G.: Causes of the Northern Gulf of Guinea Cold Event in 2012, *J Geophys Res-Oceans*, 126, e2021JC017627, <https://doi.org/10.1029/2021JC017627>, 2021.

Ding, H., Keenlyside, N. S., and Latif, M.: Seasonal cycle in the upper equatorial Atlantic Ocean, *J Geophys Res-Oceans*, 114, C09016, <https://doi.org/10.1029/2009jc005418>, 2009.

Djakouré, S., Penven, P., Bourlès, B., Kone, V., and Veitch, J.: Respective roles of the Guinea Current and local winds on the coastal upwelling in the northern Gulf of Guinea, *J Phys Oceanogr*, 47, 1367-1387, <https://doi.org/10.1175/Jpo-D-16-0126.1>, 2017.

Djakouré, S., Penven, P., Bourlès, B., Veitch, J., and Kone, V.: Coastally trapped eddies in the north of the Gulf of Guinea, *J Geophys Res-Oceans*, 119, 6805-6819, <https://doi.org/10.1002/2014jc010243>, 2014.

Duteil, O., Böning, C. W., and Oschlies, A.: Variability in subtropical-tropical cells drives oxygen levels in the tropical Pacific Ocean, *Geophys Res Lett*, 41, 8926-8934, <https://doi.org/10.1002/2014gl061774>, 2014.

1101 FAO: Fishery and Aquaculture Country Profiles. Angola. Country Profile Fact Sheets. Fisheries
 1102 and Aquaculture Division [online], Rome, 2022.
 1103 Foltz, G. R. and McPhaden, M. J.: Abrupt equatorial wave-induced cooling of the Atlantic cold
 1104 tongue in 2009, *Geophys Res Lett*, 37, <https://doi.org/10.1029/2010gl045522>, 2010a.
 1105 Foltz, G. R. and McPhaden, M. J.: Interaction between the Atlantic meridional and Nino modes,
 1106 *Geophys Res Lett*, 37, <https://doi.org/Artn L18604>
 1107 Doi 10.1029/2010gl044001, 2010b.
 1108 Foltz, G. R., Brandt, P., Richter, I., Rodriguez-Fonsecao, B., Hernandez, F., Dengler, M.,
 1109 Rodrigues, R. R., Schmidt, J. O., Yu, L., Lefevre, N., Da Cunha, L. C., McPhaden, M. J., Araujo,
 1110 M., Karstensen, J., Hahn, J., Martin-Rey, M., Patricola, C. M., Poli, P., Zuidema, P., Hummels,
 1111 R., Perez, R. C., Hatje, V., Lübbecke, J. F., Palo, I., Lumpkin, R., Bourlès, B., Asuquo, F. E.,
 1112 Lehodey, P., Conchon, A., Chang, P., Dandin, P., Schmid, C., Sutton, A., Giordani, H., Xue, Y.,
 1113 Illig, S., Losada, T., Grodsky, S. A., Gasparinss, F., Lees, T., Mohino, E., Nobre, P., Wanninkhof,
 1114 R., Keenlyside, N., Garcon, V., Sanchez-Gomez, E., Nnamchi, H. C., Drevillon, M., Storto, A.,
 1115 Remy, E., Lazar, A., Speich, S., Goes, M., Dorrington, T., Johns, W. E., Moum, J. N., Robinson,
 1116 C., Perruches, C., de Souza, R. B., Gaye, A. T., Lopez-Paragess, J., Monerie, P. A., Castellanos,
 1117 P., Benson, N. U., Houkonnou, M. N., Duha, J. T., Laxenaire, R., and Reul, N.: The Tropical
 1118 Atlantic Observing System, *Front Mar Sci*, 6, 206, <https://doi.org/10.3389/fmars.2019.00206>,
 1119 2019.
 1120 Fu, Y., Brandt, P., Tuchen, F. P., Lübbecke, J. F., and Wang, C. Z.: Representation of the mean
 1121 Atlantic subtropical cells in CMIP6 models, *J Geophys Res-Oceans*, 127, e2021JC018191,
 1122 <https://doi.org/10.1029/2021JC018191>, 2022.
 1123 Gammelsrød, T., Bartholomae, C. H., Boyer, D. C., Filipe, V. L. L., and O'Toole, M. J.: Intrusion
 1124 of warm surface water along the Angolan-Namibian coast in February-March 1995: The 1995
 1125 Benguela Niño, *S Afr J Marine Sci*, 19, 41-56, <https://doi.org/10.2989/025776198784126719>,
 1126 1998.
 1127 Garzoli, S. L. and Katz, E. J.: The Forced Annual Reversal of the Atlantic North Equatorial
 1128 Countercurrent, *J Phys Oceanogr*, 13, 2082-2090, [https://doi.org/10.1175/1520-0485\(1983\)013<2082:Tfarot>2.0.Co;2](https://doi.org/10.1175/1520-0485(1983)013<2082:Tfarot>2.0.Co;2), 1983.
 1130 Giordani, H. and Caniaux, G.: Diagnosing vertical motion in the Equatorial Atlantic, *Ocean*
 1131 *Dynam*, 61, 1995-2018, <https://doi.org/10.1007/s10236-011-0467-7>, 2011.
 1132 Grodsky, S. A., Carton, J. A., and McClain, C. R.: Variability of upwelling and chlorophyll in the
 1133 equatorial Atlantic, *Geophys Res Lett*, 35, L03610, <https://doi.org/10.1029/2007gl032466>,
 1134 2008.
 1135 Hall, R. A., Huthnance, J. M., and Williams, R. G.: Internal wave reflection on shelf slopes with
 1136 depth-varying stratification, *J Phys Oceanogr*, 43, 248-258, <https://doi.org/10.1175/Jpo-D-11-0192.1>, 2013.
 1138 Hammond, M. L., Beaulieu, C., Henson, S. A., and Sahu, S. K.: Regional surface chlorophyll
 1139 trends and uncertainties in the global ocean, *Sci Rep-Uk*, 10, 15273, <https://doi.org/10.1038/s41598-020-72073-9>, 2020.
 1141 Han, W. Q., McCreary, J. P., Masumoto, Y., Vialard, J., and Duncan, B.: Basin Resonances in the
 1142 Equatorial Indian Ocean, *J Phys Oceanogr*, 41, 1252-1270, <https://doi.org/10.1175/2011jpo4591.1>, 2011.
 1144 Hardman-Mountford, N. J. and McGlade, J. M.: Seasonal and interannual variability of
 1145 oceanographic processes in the Gulf of Guinea: an investigation using AVHRR sea surface
 1146 temperature data, *Int J Remote Sens*, 24, 3247-3268, <https://doi.org/10.1080/0143116021000021297>, 2003.
 1147

1148 Herbert, G., Bourlès, B., Penven, P., and Grelet, J.: New insights on the upper layer circulation
 1149 north of the Gulf of Guinea, *J Geophys Res-Oceans*, 121, 6793-6815, [https://doi.org/](https://doi.org/10.1002/2016jc011959)
 1150 [10.1002/2016jc011959](https://doi.org/10.1002/2016jc011959), 2016.
 1151 Herbland, A. and Voituriez, B.: Hydrological Structure-Analysis for Estimating the Primary
 1152 Production in the Tropical Atlantic Ocean, *J Mar Res*, 37, 87-101, 1979.
 1153 Heukamp, F. O., Brandt, P., Dengler, M., Tuchen, F. P., McPhaden, M. J., and Moum, J. N.:
 1154 Tropical instability waves and wind-forced cross-equatorial flow in the central Atlantic Ocean,
 1155 *Geophys Res Lett*, 49, e2022GL099325, <https://doi.org/10.1029/2022GL099325>, 2022.
 1156 Hisard, P.: El-Niño response of the eastern Tropical Atlantic, *Oceanol Acta*, 3, 69-78, 1980.
 1157 Hormann, V. and Brandt, P.: Upper equatorial Atlantic variability during 2002 and 2005
 1158 associated with equatorial Kelvin waves, *J Geophys Res-Oceans*, 114, C03007, [https://doi.org/](https://doi.org/10.1029/2008jc005101)
 1159 [10.1029/2008jc005101](https://doi.org/10.1029/2008jc005101), 2009.
 1160 Hughes, C. W., Fukumori, I., Griffies, S. M., Huthnance, J. M., Minobe, S., Spence, P.,
 1161 Thompson, K. R., and Wise, A.: Sea Level and the Role of Coastal Trapped Waves in Mediating
 1162 the Influence of the Open Ocean on the Coast, *Surv Geophys*, 40, 1467-1492, [https://doi.org/](https://doi.org/10.1007/s10712-019-09535-x)
 1163 [10.1007/s10712-019-09535-x](https://doi.org/10.1007/s10712-019-09535-x), 2019.
 1164 Hummels, R., Dengler, M., and Bourlès, B.: Seasonal and regional variability of upper ocean
 1165 diapycnal heat flux in the Atlantic cold tongue, *Prog Oceanogr*, 111, 52-74, [https://doi.org/](https://doi.org/10.1016/j.pocean.2012.11.001)
 1166 [10.1016/j.pocean.2012.11.001](https://doi.org/10.1016/j.pocean.2012.11.001), 2013.
 1167 Hummels, R., Dengler, M., Brandt, P., and Schlundt, M.: Diapycnal heat flux and mixed layer
 1168 heat budget within the Atlantic Cold Tongue, *Clim Dynam*, 43, 3179-3199, [https://doi.org/](https://doi.org/10.1007/s00382-014-2339-6)
 1169 [10.1007/s00382-014-2339-6](https://doi.org/10.1007/s00382-014-2339-6), 2014.
 1170 Hutchings, L., van der Lingen, C. D., Shannon, L. J., Crawford, R. J. M., Verheye, H. M. S.,
 1171 Bartholomae, C. H., van der Plas, A. K., Louw, D., Kreiner, A., Ostrowski, M., Fidel, Q., Barlow,
 1172 R. G., Lamont, T., Coetzee, J., Shillington, F., Veitch, J., Currie, J. C., and Monteiro, P. M. S.: The
 1173 Benguela Current: An ecosystem of four components, *Prog Oceanogr*, 83, 15-32, [https://doi.](https://doi.org/10.1016/j.pocean.2009.07.046)
 1174 [org/10.1016/j.pocean.2009.07.046](https://doi.org/10.1016/j.pocean.2009.07.046), 2009.
 1175 Illig, S., Bachèlery, M. L., and Cadier, E.: Subseasonal coastal-trapped wave propagations in the
 1176 southeastern Pacific and Atlantic oceans: 2. Wave characteristics and connection with the
 1177 equatorial variability, *J Geophys Res-Oceans*, 123, 3942-3961, [https://doi.org/](https://doi.org/10.1029/2017jc013540)
 1178 [10.1029/2017jc013540](https://doi.org/10.1029/2017jc013540), 2018a.
 1179 Illig, S., Cadier, E., Bachèlery, M. L., and Kersale, M.: Subseasonal coastal-trapped wave
 1180 propagations in the southeastern Pacific and Atlantic oceans: 1. A new approach to estimate
 1181 wave amplitude, *J Geophys Res-Oceans*, 123, 3915-3941, [https://doi.org/](https://doi.org/10.1029/2017jc013539)
 1182 [10.1029/2017jc013539](https://doi.org/10.1029/2017jc013539), 2018b.
 1183 Illig, S., Dewitte, B., Ayoub, N., du Penhoat, Y., Reverdin, G., De Mey, P., Bonjean, F., and
 1184 Lagerloef, G. S. E.: Interannual long equatorial waves in the tropical Atlantic from a high-
 1185 resolution ocean general circulation model experiment in 1981-2000, *J Geophys Res-Oceans*,
 1186 109, C02022, <https://doi.org/10.1029/2003jc001771>, 2004.
 1187 Imbol Koungue, R. A. and Brandt, P.: Impact of intraseasonal waves on Angolan warm and cold
 1188 events, *J Geophys Res-Oceans*, 126, e2020JC017088, <https://doi.org/10.1029/2020JC017088>,
 1189 2021.
 1190 Imbol Koungue, R. A., Illig, S., and Rouault, M.: Role of interannual Kelvin wave propagations
 1191 in the equatorial Atlantic on the Angola Benguela Current system, *J Geophys Res-Oceans*, 122,
 1192 4685-4703, <https://doi.org/10.1002/2016jc012463>, 2017.
 1193 Imbol Koungue, R. A., Rouault, M., Illig, S., Brandt, P., and Jouanno, J.: Benguela Niños and
 1194 Benguela Niñas in Forced Ocean Simulation From 1958 to 2015, *J Geophys Res-Oceans*, 124,
 1195 5923-5951, <https://doi.org/10.1029/2019jc015013>, 2019.

1196 Imbol Koungue, R. A., Brandt, P., Lübbecke, J. F., Prigent, A., Sena Martins, M., and Rodrigues,
 1197 R. R.: The 2019 Benguela Niño, *Front Mar Sci*, 8, 800103, [https://doi.org/](https://doi.org/10.3389/fmars.2021.800103)
 1198 10.3389/fmars.2021.800103, 2021.
 1199 Ingham, M. C.: Coastal upwelling in northwestern Gulf of Guinea, *B Mar Sci*, 20, 1-34, 1970.
 1200 Johns, W. E., Brandt, P., Bourlès, B., Tantet, A., Papapostolou, A., and Houk, A.: Zonal structure
 1201 and seasonal variability of the Atlantic Equatorial Undercurrent, *Clim Dynam*, 43, 3047-3069,
 1202 <https://doi.org/10.1007/s00382-014-2136-2>, 2014.
 1203 Jouanno, J., Hernandez, O., and Sanchez-Gomez, E.: Equatorial Atlantic interannual variability
 1204 and its relation to dynamic and thermodynamic processes, *Earth Syst Dynam*, 8, 1061-1069,
 1205 <https://doi.org/10.5194/esd-8-1061-2017>, 2017.
 1206 Jouanno, J., Marin, F., du Penhoat, Y., and Molines, J. M.: Intraseasonal modulation of the
 1207 surface cooling in the Gulf of Guinea, *J Phys Oceanogr*, 43, 382-401, [https://doi.org/](https://doi.org/10.1175/Jpo-D-12-053.1)
 1208 10.1175/Jpo-D-12-053.1, 2013.
 1209 Jouanno, J., Marin, F., du Penhoat, Y., Molines, J. M., and Sheinbaum, J.: Seasonal modes of
 1210 surface cooling in the Gulf of Guinea, *J Phys Oceanogr*, 41, 1408-1416, [https://doi.org/](https://doi.org/10.1175/Jpo-D-11-031.1)
 1211 10.1175/Jpo-D-11-031.1, 2011a.
 1212 Jouanno, J., Marin, F., du Penhoat, Y., Sheinbaum, J., and Molines, J. M.: Seasonal heat balance
 1213 in the upper 100 m of the equatorial Atlantic Ocean, *J Geophys Res-Oceans*, 116, C09003,
 1214 <https://doi.org/10.1029/2010jc006912>, 2011b.
 1215 Kämpf, J.: On the magnitude of upwelling fluxes in shelf-break canyons, *Cont Shelf Res*, 27,
 1216 2211-2223, <https://doi.org/10.1016/j.csr.2007.05.010>, 2007.
 1217 Katz, E. J. and Garzoli, S.: Response of the western Equatorial Atlantic Ocean to an annual wind
 1218 cycle, *J Mar Res*, 40, 307-327, 1982.
 1219 Keenlyside, N. S. and Latif, M.: Understanding equatorial Atlantic interannual variability, *J*
 1220 *Climate*, 20, 131-142, <https://doi.org/10.1175/Jcli3992.1>, 2007.
 1221 Kiko, R., Biastoch, A., Brandt, P., Cravatte, S., Hauss, H., Hummels, R., Kriest, I., Marin, F.,
 1222 McDonnell, A. M. P., Oschlies, A., Picheral, M., Schwarzkopf, F. U., Thurnherr, A. M., and
 1223 Stemmann, L.: Biological and physical influences on marine snowfall at the equator, *Nat*
 1224 *Geosci*, 10, 852-858, <https://doi.org/10.1038/Ngeo3042>, 2017.
 1225 Knight, J. R., Folland, C. K., and Scaife, A. A.: Climate impacts of the Atlantic Multidecadal
 1226 Oscillation, *Geophys Res Lett*, 33, L17706, <https://doi.org/10.1029/2006gl026242>, 2006.
 1227 Kolodziejczyk, N., Marin, F., Bourlès, B., Gouriou, Y., and Berger, H.: Seasonal variability of the
 1228 equatorial undercurrent termination and associated salinity maximum in the Gulf of Guinea,
 1229 *Clim Dynam*, 43, 3025-3046, <https://doi.org/10.1007/s00382-014-2107-7>, 2014.
 1230 Koné, V., Lett, C., Penven, P., Bourles, B., and Djakouré, S.: A biophysical model of *S. aurita*
 1231 early life history in the northern Gulf of Guinea, *Prog Oceanogr*, 151, 83-96, [https://doi.org/](https://doi.org/10.1016/j.pocean.2016.10.008)
 1232 10.1016/j.pocean.2016.10.008, 2017.
 1233 Kopte, R., Brandt, P., Claus, M., Greatbatch, R. J., and Dengler, M.: Role of equatorial basin-
 1234 mode resonance for the seasonal variability of the Angola Current at 11°S, *J Phys Oceanogr*,
 1235 48, 261-281, <https://doi.org/10.1175/Jpo-D-17-0111.1>, 2018.
 1236 Kopte, R., Brandt, P., Dengler, M., Tchikalanga, P. C. M., Macueria, M., and Ostrowski, M.: The
 1237 Angola Current: Flow and hydrographic characteristics as observed at 11°S, *J Geophys Res-*
 1238 *Oceans*, 122, 1177-1189, <https://doi.org/10.1002/2016jc012374>, 2017.
 1239 Körner, M., Brandt, P., and Dengler, M.: Seasonal cycle of sea surface temperature in the
 1240 tropical Angolan upwelling system, *EGUsphere*, 1-33, [https://doi.org/10.5194/egusphere-](https://doi.org/10.5194/egusphere-2022-973)
 1241 2022-973, 2022.

1242 Lamb, K. G.: Internal wave breaking and dissipation mechanisms on the continental
 1243 slope/shelf, *Annu Rev Fluid Mech*, 46, 231-254, [https://doi.org/10.1146/annurev-fluid-](https://doi.org/10.1146/annurev-fluid-011212-140701)
 1244 [011212-140701](https://doi.org/10.1146/annurev-fluid-011212-140701), 2014.
 1245 Longhurst, A.: Seasonal cooling and blooming in tropical oceans, *Deep-Sea Res Pt I*, 40, 2145-
 1246 2165, [https://doi.org/10.1016/0967-0637\(93\)90095-K](https://doi.org/10.1016/0967-0637(93)90095-K), 1993.
 1247 Loukos, H. and Memery, L.: Simulation of the nitrate seasonal cycle in the equatorial Atlantic
 1248 Ocean during 1983 and 1984, *J Geophys Res-Oceans*, 104, 15549-15573, [https://doi.org/](https://doi.org/10.1029/1999jc900084)
 1249 [10.1029/1999jc900084](https://doi.org/10.1029/1999jc900084), 1999.
 1250 Lübbecke, J. F., Rodriguez-Fonseca, B., Richter, I., Martin-Rey, M., Losada, T., Polo, I., and
 1251 Keenlyside, N. S.: Equatorial Atlantic variability—Modes, mechanisms, and global
 1252 teleconnections, *Wires Clim Change*, 9, e527, <https://doi.org/10.1002/wcc.527>, 2018.
 1253 Lübbecke, J. F., Brandt, P., Dengler, M., Koppe, R., Ludke, J., Richter, I., Martins, M. S., and
 1254 Tchikalanga, P. C. M.: Causes and evolution of the southeastern tropical Atlantic warm event
 1255 in early 2016, *Clim Dynam*, 53, 261-274, <https://doi.org/10.1007/s00382-018-4582-8>, 2019.
 1256 Mao, Z. X., Mao, Z. H., Jamet, C., Linderman, M., Wang, Y. T., and Chen, X. Y.: Seasonal Cycles
 1257 of Phytoplankton Expressed by Sine Equations Using the Daily Climatology from Satellite-
 1258 Retrieved Chlorophyll-a Concentration (1997-2019) Over Global Ocean, *Remote Sens-Basel*,
 1259 12, 2662, <https://doi.org/10.3390/rs12162662>, 2020.
 1260 Marchal, E. and Picaut, J.: Répartition et abondance évaluées par échantillonnage des poissons
 1261 du plateau ivoiro-ghanéen en relation avec les upwellings locaux, *J Rech Océanogr*, 2, 39-58,
 1262 1977.
 1263 Marchesiello, P. and Estrade, P.: Upwelling limitation by onshore geostrophic flow, *J Mar Res*,
 1264 68, 37-62, <https://doi.org/10.1357/002224010793079004>, 2010.
 1265 Martins, M. S. and Stammer, D.: Interannual variability of the Congo River plume-induced sea
 1266 surface salinity, *Remote Sens-Basel*, 14, 1013, <https://doi.org/10.3390/rs14041013>, 2022.
 1267 Menkes, C. E., Kennan, S. C., Flament, P., Dandonneau, Y., Masson, S., Biessy, B., Marchal, E.,
 1268 Eldin, G., Grelet, J., Montel, Y., Morliere, A., Lebourges-Dhaussy, A., Moulin, C., Champalbert,
 1269 G., and Herbland, A.: A whirling ecosystem in the equatorial Atlantic, *Geophys Res Lett*, 29,
 1270 1553, <https://doi.org/10.1029/2001gl014576>, 2002.
 1271 Merle, J.: Seasonal Heat-Budget in the Equatorial Atlantic-Ocean, *J Phys Oceanogr*, 10, 464-
 1272 469, [https://doi.org/10.1175/1520-0485\(1980\)010<0464:Shbite>2.0.Co;2](https://doi.org/10.1175/1520-0485(1980)010<0464:Shbite>2.0.Co;2), 1980.
 1273 Monger, B., McClain, C., and Murtugudde, R.: Seasonal phytoplankton dynamics in the eastern
 1274 tropical Atlantic, *J Geophys Res-Oceans*, 102, 12389-12411, [https://doi.org/](https://doi.org/10.1029/96jc03982)
 1275 [10.1029/96jc03982](https://doi.org/10.1029/96jc03982), 1997.
 1276 Moore, D., Hisard, P., McCreary, J., Merle, J., O'Brien, J., Picaut, J., Verstraete, J. M., and
 1277 Wunsch, C.: Equatorial adjustment in the eastern Atlantic, *Geophys Res Lett*, 5, 637-640,
 1278 <https://doi.org/10.1029/GL005i008p00637>, 1978.
 1279 Moore, J. K., Doney, S. C., and Lindsay, K.: Upper ocean ecosystem dynamics and iron cycling
 1280 in a global three-dimensional model, *Global Biogeochem Cy*, 18, Gb4028, [https://doi.org/](https://doi.org/10.1029/2004gb002220)
 1281 [10.1029/2004gb002220](https://doi.org/10.1029/2004gb002220), 2004.
 1282 Mosquera-Vasquez, K., Dewitte, B., and Illig, S.: The Central Pacific El Nino intraseasonal Kelvin
 1283 wave, *J Geophys Res-Oceans*, 119, 6605-6621, <https://doi.org/10.1002/2014jc010044>, 2014.
 1284 Moum, J. N., Lien, R. C., Perlin, A., Nash, J. D., Gregg, M. C., and Wiles, P. J.: Sea surface cooling
 1285 at the Equator by subsurface mixing in tropical instability waves, *Nat Geosci*, 2, 761-765,
 1286 <https://doi.org/10.1038/Ngeo657>, 2009.
 1287 Moum, J. N., Hughes, K. G., Shroyer, E. L., Smyth, W. D., Cherian, D., Warner, S. J., Bourles, B.,
 1288 Brandt, P., and Dengler, M.: Deep Cycle Turbulence in Atlantic and Pacific Cold Tongues,
 1289 *Geophys Res Lett*, 49, e2021GL097345, <https://doi.org/10.1029/2021GL097345>, 2022.

1290 Nnamchi, H. C., Li, J. P., Kucharski, F., Kang, I. S., Keenlyside, N. S., Chang, P., and Farneti, R.:
 1291 Thermodynamic controls of the Atlantic Nino, *Nat Commun*, 6, 8895, [https://doi.org/](https://doi.org/10.1038/ncomms9895)
 1292 10.1038/ncomms9895, 2015.
 1293 Nyadjro, E. S., Foli, B. A. K., Agyekum, K. A., Wiafe, G., and Tsei, S.: Seasonal Variability of Sea
 1294 Surface Salinity in the NW Gulf of Guinea from SMAP Satellite, *Remote Sens Earth Syst Sci*, 5,
 1295 83-94, <https://doi.org/10.1007/s41976-021-00061-2>, 2022.
 1296 Okumura, Y. and Xie, S. P.: Some overlooked features of tropical Atlantic climate leading to a
 1297 new Nino-like phenomenon, *J Climate*, 19, 5859-5874, <https://doi.org/10.1175/Jcli3928.1>,
 1298 2006.
 1299 Oschlies, A., Brandt, P., Stramma, L., and Schmidtko, S.: Drivers and mechanisms of ocean
 1300 deoxygenation, *Nat Geosci*, 11, 467-473, <https://doi.org/10.1038/s41561-018-0152-2>, 2018.
 1301 Ostrowski, M., da Silva, J. C. B., and Bazik-Sangolay, B.: The response of sound scatterers to El
 1302 Niño- and La Niña-like oceanographic regimes in the southeastern Atlantic, *Ices J Mar Sci*, 66,
 1303 1063-1072, <https://doi.org/10.1093/icesjms/fsp102>, 2009.
 1304 Perez, R. C., Hormann, V., Lumpkin, R., Brandt, P., Johns, W. E., Hernandez, F., Schmid, C., and
 1305 Bourlès, B.: Mean meridional currents in the central and eastern equatorial Atlantic, *Clim*
 1306 *Dynam*, 43, 2943-2962, <https://doi.org/10.1007/s00382-013-1968-5>, 2014.
 1307 Perlin, A., Moum, J. N., and Klymak, J. M.: Response of the bottom boundary layer over a
 1308 sloping shelf to variations in alongshore wind, *J Geophys Res-Oceans*, 110, C10S09, [https://](https://doi.org/10.1029/2004jc002500)
 1309 doi.org/10.1029/2004jc002500, 2005.
 1310 Philander, S. G. H.: Upwelling in the Gulf of Guinea, *J Mar Res*, 37, 23-33, 1979.
 1311 Philander, S. G. H. and Pacanowski, R. C.: Response of equatorial oceans to periodic forcing, *J*
 1312 *Geophys Res-Oc Atm*, 86, 1903-1916, <https://doi.org/10.1029/Jc086ic03p01903>, 1981.
 1313 Philander, S. G. H. and Pacanowski, R. C.: A model of the seasonal cycle in the tropical Atlantic-
 1314 Ocean, *J Geophys Res-Oceans*, 91, 14192-14206, <https://doi.org/10.1029/JC091ic12p14192>,
 1315 1986.
 1316 Picaut, J.: Propagation of the Seasonal Upwelling in the Eastern Equatorial Atlantic, *J Phys*
 1317 *Oceanogr*, 13, 18-37, [https://doi.org/10.1175/1520-0485\(1983\)013<0018:Potsui>2.0.Co;2](https://doi.org/10.1175/1520-0485(1983)013<0018:Potsui>2.0.Co;2),
 1318 1983.
 1319 Polo, I., Lazar, A., Rodriguez-Fonseca, B., and Arnault, S.: Oceanic Kelvin waves and tropical
 1320 Atlantic intraseasonal variability: 1. Kelvin wave characterization, *J Geophys Res-Oceans*, 113,
 1321 C07009, <https://doi.org/10.1029/2007jc004495>, 2008.
 1322 Prigent, A., Imbol Koungue, R. A., Lübbecke, J. F., Brandt, P., and Latif, M.: Origin of weakened
 1323 interannual sea surface temperature variability in the southeastern tropical Atlantic Ocean,
 1324 *Geophys Res Lett*, 47, e2020GL089348, <https://doi.org/10.1029/2020GL089348>, 2020a.
 1325 Prigent, A., Lübbecke, J. F., Bayr, T., Latif, M., and Wengel, C.: Weakened SST variability in the
 1326 tropical Atlantic Ocean since 2000, *Clim Dynam*, 54, 2731-2744, [https://doi.org/](https://doi.org/10.1007/s00382-020-05138-0)
 1327 10.1007/s00382-020-05138-0, 2020b.
 1328 Rabe, B., Schott, F. A., and Köhl, A.: Mean circulation and variability of the tropical Atlantic
 1329 during 1952-2001 in the GECCO assimilation fields, *J Phys Oceanogr*, 38, 177-192, [https://doi.](https://doi.org/10.1175/2007jpo3541.1)
 1330 [org/10.1175/2007jpo3541.1](https://doi.org/10.1175/2007jpo3541.1), 2008.
 1331 Radenac, M. H., Jouanno, J., Tchamabi, C. C., Awo, M., Bourles, B., Arnault, S., and Aumont,
 1332 O.: Physical drivers of the nitrate seasonal variability in the Atlantic cold tongue,
 1333 *Biogeosciences*, 17, 529-545, <https://doi.org/10.5194/bg-17-529-2020>, 2020.
 1334 Richter, I., Behera, S. K., Masumoto, Y., Taguchi, B., Komori, N., and Yamagata, T.: On the
 1335 triggering of Benguela Niños: Remote equatorial versus local influences, *Geophys Res Lett*, 37,
 1336 L20604, <https://doi.org/10.1029/2010gl044461>, 2010.

1337 Roch, M., Brandt, P., Schmidtke, S., Vaz Velho, F., and Ostrowski, M.: Southeastern tropical
 1338 Atlantic changing from subtropical to tropical conditions, *Front Mar Sci*, 8, 748383, <https://doi.org/10.3389/fmars.2021.748383>, 2021.
 1339
 1340 Rossi, V., Feng, M., Pattiaratchi, C., Roughan, M., and Waite, A. M.: On the factors influencing
 1341 the development of sporadic upwelling in the Leeuwin Current system, *J Geophys Res-Oceans*,
 1342 118, 3608-3621, <https://doi.org/10.1002/jgrc.20242>, 2013.
 1343 Rouault, M.: Bi-annual intrusion of tropical water in the northern Benguela upwelling,
 1344 *Geophys Res Lett*, 39, L12606, <https://doi.org/10.1029/2012gl052099>, 2012.
 1345 Rouault, M., Illig, S., Lübbecke, J. F., and Imbol Koungue, R. A.: Origin, development and
 1346 demise of the 2010-2011 Benguela Niño, *J Marine Syst*, 188, 39-48, <https://doi.org/10.1016/j.jmarsys.2017.07.007>, 2018.
 1347
 1348 Rouault, M., Illig, S., Bartholomae, C., Reason, C. J. C., and Bentamy, A.: Propagation and origin
 1349 of warm anomalies in the Angola Benguela upwelling system in 2001, *J Marine Syst*, 68, 473-
 1350 488, <https://doi.org/10.1016/j.jmarsys.2006.11.010>, 2007.
 1351 Ruiz-Barradas, A., Carton, J. A., and Nigam, S.: Structure of interannual-to-decadal climate
 1352 variability in the tropical Atlantic sector, *J Climate*, 13, 3285-3297, [https://doi.org/10.1175/1520-0442\(2000\)013<3285:Soitdc>2.0.Co;2](https://doi.org/10.1175/1520-0442(2000)013<3285:Soitdc>2.0.Co;2), 2000.
 1353
 1354 Sallee, J. B., Pellichero, V., Akhondas, C., Pauthenet, E., Vignes, L., Schmidtke, S., Garabato, A.
 1355 N., Sutherland, P., and Kuusela, M.: Summertime increases in upper-ocean stratification and
 1356 mixed-layer depth, *Nature*, 591, 592-598, <https://doi.org/10.1038/s41586-021-03303-x>,
 1357 2021.
 1358 Schafstall, J., Dengler, M., Brandt, P., and Bange, H.: Tidal-induced mixing and diapycnal
 1359 nutrient fluxes in the Mauritanian upwelling region, *J Geophys Res-Oceans*, 115, C10014,
 1360 <https://doi.org/10.1029/2009jc005940>, 2010.
 1361 Schott, F. A., Fischer, J., and Stramma, L.: Transports and pathways of the upper-layer
 1362 circulation in the western tropical Atlantic, *J Phys Oceanogr*, 28, 1904-1928, [https://doi.org/10.1175/1520-0485\(1998\)028<1904:TAPOTU>2.0.CO;2](https://doi.org/10.1175/1520-0485(1998)028<1904:TAPOTU>2.0.CO;2), 1998.
 1363
 1364 Schott, F. A., McCreary, J. P., and Johnson, G. C.: Shallow overturning circulations of the
 1365 tropical-subtropical oceans, in: *Earth Climate: The Ocean-Atmosphere Interaction*, edited by:
 1366 Wang, C., Xie, S.-P., and Carton, J. A., Geophysical Monograph 147, American Geophysical
 1367 Union, Washington, DC, 261-304, <https://doi.org/10.1029/147GM15>, 2004.
 1368 Servain, J., Picaut, J., and Merle, J.: Evidence of Remote Forcing in the Equatorial Atlantic-
 1369 Ocean, *J Phys Oceanogr*, 12, 457-463, [https://doi.org/10.1175/1520-0485\(1982\)012<0457:Eorfit>2.0.Co;2](https://doi.org/10.1175/1520-0485(1982)012<0457:Eorfit>2.0.Co;2), 1982.
 1370
 1371 Shannon, L. V., Boyd, A. J., Brundrit, G. B., and Taunton-Clark, J.: On the Existence of an El-
 1372 Niño-Type Phenomenon in the Benguela System, *J Mar Res*, 44, 495-520, <https://doi.org/10.1357/002224086788403105>, 1986.
 1373
 1374 Sherman, J., Subramaniam, A., Gorbunov, M. Y., Fernandez-Carrera, A., Kiko, R., Brandt, P.,
 1375 and Falkowski, P. G.: The photophysiological response of nitrogen-limited phytoplankton to
 1376 episodic nitrogen supply associated with Tropical Instability Waves in the equatorial Atlantic,
 1377 *Front Mar Sci*, 8, 814663, <https://doi.org/10.3389/fmars.2021.814663>, 2022.
 1378 Siegfried, L., Schmidt, M., Mohrholz, V., Pogrzeba, H., Nardini, P., Böttlinger, M., and
 1379 Scheuermann, G.: The tropical-subtropical coupling in the Southeast Atlantic from the
 1380 perspective of the northern Benguela upwelling system, *Plos One*, 14, e0210083, <https://doi.org/10.1371/journal.pone.0210083>, 2019.
 1381
 1382 Sohau, Z., Koné, V., Da-Allada, Y. C., Djakouré, S., Bourlès, B., Racape, V., Degbe, G., and Adje,
 1383 C.: Seasonal and inter-annual ONSET Sea Surface Temperature variability along the northern

coast of the Gulf of Guinea, *Reg Stud Mar Sci*, 35, 101129, <https://doi.org/10.1016/j.rsma.2020.101129>, 2020.

Sowman, M. and Cardoso, P.: Small-scale fisheries and food security strategies in countries in the Benguela Current Large Marine Ecosystem (BCLME) region: Angola, Namibia and South Africa, *Marine Policy*, 34, 1163-1170, <https://doi.org/10.1016/j.marpol.2010.03.016>, 2010.

Tchupalanga, P., Dengler, M., Brandt, P., Kopte, R., Macueria, M., Coelho, P., Ostrowski, M., and Keenlyside, N. S.: Eastern Boundary Circulation and Hydrography Off Angola: Building Angolan Oceanographic Capacities, *B Am Meteorol Soc*, 99, 1589-1605, <https://doi.org/10.1175/Bams-D-17-0197.1>, 2018.

Thomsen, S., Capet, X., and Echevin, V.: Competition between Baroclinic Instability and Ekman Transport under Varying Buoyancy Forcings in Upwelling Systems: An Idealized Analog to the Southern Ocean, *J Phys Oceanogr*, 51, 3347-3364, <https://doi.org/10.1175/Jpo-D-20-0294.1>, 2021.

Thomsen, S., Kanzow, T., Krahmann, G., Greatbatch, R. J., Dengler, M., and Lavik, G.: The formation of a subsurface anticyclonic eddy in the Peru-Chile Undercurrent and its impact on the near-coastal salinity, oxygen, and nutrient distributions, *J Geophys Res-Oceans*, 121, 476-501, <https://doi.org/10.1002/2015jc010878>, 2016.

Tokinaga, H. and Xie, S. P.: Weakening of the equatorial Atlantic cold tongue over the past six decades, *Nat Geosci*, 4, 222-226, <https://doi.org/10.1038/Ngeo1078>, 2011.

Toualy, E., Kouacou, B., and Aman, A.: Influence of Wind and Surface Buoyancy Flux on the Variability of the Oceanic Mixed Layer Depth in the Northern Gulf of Guinea Coastal Upwelling, *Thalassas*, 38, 599-608, <https://doi.org/10.1007/s41208-021-00358-5>, 2022.

Tuchen, F. P., Brandt, P., Lübbecke, J. F., and Hummels, R.: Transports and pathways of the tropical AMOC return flow from Argo data and shipboard velocity measurements, *J Geophys Res-Oceans*, 127, e2021JC018115, <https://doi.org/10.1029/2021JC018115>, 2022a.

Tuchen, F. P., Lübbecke, J. F., Brandt, P., and Fu, Y.: Observed transport variability of the Atlantic Subtropical Cells and their connection to tropical sea surface temperature variability, *J Geophys Res-Oceans*, 125, e2020JC016592, <https://doi.org/10.1029/2020JC016592>, 2020.

Tuchen, F. P., Lübbecke, J. F., Schmidtko, S., Hummels, R., and Böning, C. W.: The Atlantic Subtropical Cells Inferred from Observations, *J Geophys Res-Oceans*, 124, 7591-7605, <https://doi.org/10.1029/2019jc015396>, 2019.

Tuchen, F. P., Perez, R. C., Foltz, G. R., Brandt, P., and Lumpkin, R.: Multidecadal intensification of Atlantic tropical instability waves, *Geophys Res Lett*, 49, e2022GL101073, <https://doi.org/10.1029/2022GL101073>, 2022b.

Voituriez, B., Herbland, A., and Le Borgne, R.: L'upwelling équatorial de l'Atlantique Est pendant l'Expérience Météorologique Mondiale (PEMG), *Oceanol Acta*, 5, 301-314, 1982.

Wade, M., Caniaux, G., and du Penhoat, Y.: Variability of the mixed layer heat budget in the eastern equatorial Atlantic during 2005-2007 as inferred using Argo floats, *J Geophys Res-Oceans*, 116, C08006, <https://doi.org/10.1029/2010jc006683>, 2011.

Wang, D. W., Gouhier, T. C., Menge, B. A., and Ganguly, A. R.: Intensification and spatial homogenization of coastal upwelling under climate change, *Nature*, 518, 390-394, <https://doi.org/10.1038/nature14235>, 2015.

Warner, S. J., Holmes, R. M., Hawkins, E. H. M., Hoecker-Martinez, M. S., Savage, A. C., and Moum, J. N.: Buoyant gravity currents released from Tropical Instability Waves, *J Phys Oceanogr*, 48, 361-382, <https://doi.org/10.1175/Jpo-D-17-0144.1>, 2018.

Weingartner, T. J. and Weisberg, R. H.: On the Annual Cycle of Equatorial Upwelling in the Central Atlantic-Ocean, *J Phys Oceanogr*, 21, 68-82, [https://doi.org/10.1175/1520-0485\(1991\)021<0068:Otacoe>2.0.Co;2](https://doi.org/10.1175/1520-0485(1991)021<0068:Otacoe>2.0.Co;2), 1991.

1432 Wiafe, G. and Nyadjro, E. S.: Satellite Observations of Upwelling in the Gulf of Guinea, *IEEE*
 1433 *Geosci Remote S*, 12, 1066-1070, <https://doi.org/10.1109/Lgrs.2014.2379474>, 2015.
 1434 Yang, H., Lohmann, G., Krebs-Kanzow, U., Ionita, M., Shi, X. X., Sidorenko, D., Gong, X., Chen,
 1435 X. E., and Gowan, E. J.: Poleward Shift of the Major Ocean Gyres Detected in a Warming
 1436 Climate, *Geophys Res Lett*, 47, e2019GL085868, <https://doi.org/10.1029/2019GL085868>,
 1437 2020.
 1438 Yang, Y., Wu, L. X., Cai, W. J., Jia, F., Ng, B., Wang, G. J., and Geng, T.: Suppressed Atlantic
 1439 Nino/Nina variability under greenhouse warming, *Nat Clim Change*, 12, 814-821, [https://doi.](https://doi.org/10.1038/s41558-022-01444-z)
 1440 [org/10.1038/s41558-022-01444-z](https://doi.org/10.1038/s41558-022-01444-z), 2022.
 1441 Zeng, Z., Brandt, P., Lamb, K. G., Greatbatch, R. J., Dengler, M., Claus, M., and Chen, X.: Three-
 1442 dimensional numerical simulations of internal tides in the Angolan upwelling region, *J*
 1443 *Geophys Res-Oceans*, 126, e2020JC016460, <https://doi.org/10.1029/2020JC016460>, 2021.
 1444